

**A peer-reviewed version of this preprint was published in PeerJ on 22 August 2018.**

[View the peer-reviewed version](https://doi.org/10.7717/peerj.5457) (peerj.com/articles/5457), which is the preferred citable publication unless you specifically need to cite this preprint.

Hengl T, Walsh MG, Sanderman J, Wheeler I, Harrison SP, Prentice IC. 2018. Global mapping of potential natural vegetation: an assessment of machine learning algorithms for estimating land potential. PeerJ 6:e5457 <https://doi.org/10.7717/peerj.5457>

# Global mapping of potential natural vegetation: an assessment of Machine Learning algorithms for estimating land potential

Tomislav Hengl<sup>Corresp., 1</sup>, Markus G Walsh<sup>2</sup>, Jonathan Sanderman<sup>3</sup>, Ichsani Wheeler<sup>4</sup>, Sandy P Harrison<sup>5</sup>, Iain C Prentice<sup>6</sup>

<sup>1</sup> Envirometrix Ltd, Wageningen, The Netherlands

<sup>2</sup> The Earth Institute, Columbia University, New York, United States

<sup>3</sup> Woods Hole Research Center, Falmouth, United States

<sup>4</sup> Envirometrix, Wageningen, The Netherlands

<sup>5</sup> University of Reading, Reading, United Kingdom

<sup>6</sup> Department of Life Sciences and Grantham Institute - Climate Change and the Environment, Imperial College London, London, United Kingdom

Corresponding Author: Tomislav Hengl

Email address: tom.hengl@gmail.com

Potential Natural Vegetation (PNV) is the vegetation cover in equilibrium with climate, that would exist at a given location non-impacted by human activities. PNV is useful for raising public awareness about land degradation and for estimating land potential. This paper presents results of assessing Machine Learning Algorithms (MLA) for operational mapping of Potential Natural Vegetation (PNV). The following MLA were considered: neural networks (nnet package), random forest (ranger), gradient boosting (gmb), K-nearest neighborhood (class) and cubist. Three case studies were considered: (1) global distribution of biomes based on the BIOME 6000 data set (8057 modern pollen-based site reconstructions), (2) distribution of forest tree taxa in Europe based on detailed occurrence records (1,546,435 ground observations), and (3) global monthly Fraction of Absorbed Photosynthetically Active Radiation (FAPAR) values (30,301 randomly-sampled points). A stack of 160 global maps representing biophysical conditions over land, including atmospheric, climatic, relief and lithologic variables, were used as explanatory variables. The overall results show that random forest gives the overall best performance. The highest accuracy for predicting BIOME 6000 classes (20) was estimated at 68% (33% with spatial Cross Validation) with the most important predictors being total annual precipitation, monthly temperatures and bioclimatic layers. Predicting forest tree species (73) resulted in mapping accuracy of 25%, with the most important predictors being monthly cloud fraction, mean annual and monthly temperatures and elevation. Regression models for FAPAR (monthly images) gave an R-square of 90% with most important predictors being total annual precipitation, monthly cloud fraction, CHELSA bioclimatic layers and month of the year, respectively.

Further developments of PNV mapping could include using GBIF records to map global distribution of plant species at different taxonomic levels. This methodology could also be extended to dynamic modeling of PNV, so that future climate scenarios can be incorporated. Global maps of biomes, FAPAR and tree species at 1 km spatial resolution are available for download via <http://dx.doi.org/10.7910/DVN/QQHCIK>.

# 1 **Global Mapping of Potential Natural** 2 **Vegetation: An Assessment of Machine** 3 **Learning Algorithms for Estimating Land** 4 **Potential**

5 **Tomislav Hengl<sup>1</sup>, Markus G. Walsh<sup>2</sup>, Jonathan Sanderman<sup>3</sup>, Ichsani**  
6 **Wheeler<sup>1</sup>, Sandy P. Harrison<sup>4</sup>, and I. Colin Prentice<sup>5</sup>**

7 <sup>1</sup>**Envirometrix Ltd., Wageningen, the Netherlands**

8 <sup>2</sup>**The Earth Institute, Columbia University, USA / Selian Agricultural Research Inst.,**  
9 **Arusha, Tanzania**

10 <sup>3</sup>**Woods Hole Research Center, MA USA**

11 <sup>4</sup>**School of Archeology, Geography and Environmental Science, University of Reading,**  
12 **UK**

13 <sup>5</sup>**AXA Chair of Biosphere and Climate Impacts, Grand Challenges in Ecosystem and the**  
14 **Environment, Department of Life Sciences and Grantham Institute — Climate Change**  
15 **and the Environment, Imperial College London, UK**

16 Corresponding author:

17 Tomislav Hengl<sup>1</sup>

18 Email address: tom.hengl@envirometrix.net

## 19 **ABSTRACT**

Potential Natural Vegetation (PNV) is the vegetation cover in equilibrium with climate, that would exist at a given location non-impacted by human activities. PNV is useful for raising public awareness about land degradation and for estimating land potential. This paper presents results of assessing Machine Learning Algorithms (MLA) for operational mapping of Potential Natural Vegetation (PNV). The following MLA were considered: neural networks (nnet package), random forest (ranger), gradient boosting (gmb), K-nearest neighborhood (class) and cubist. Three case studies were considered: (1) global distribution of biomes based on the BIOME 6000 data set (8057 modern pollen-based site reconstructions), (2) distribution of forest tree taxa in Europe based on detailed occurrence records (1,546,435 ground observations), and (3) global monthly Fraction of Absorbed Photosynthetically Active Radiation (FAPAR) values (30,301 randomly-sampled points). A stack of 160 global maps representing biophysical conditions over land, including atmospheric, climatic, relief and lithologic variables, were used as explanatory variables. The overall results show that random forest gives the overall best performance. The highest accuracy for predicting BIOME 6000 classes (20) was estimated at 68 % (33 % with spatial Cross Validation) with the most important predictors being total annual precipitation, monthly temperatures and bioclimatic layers. Predicting forest tree species (73) resulted in mapping accuracy of 25 %, with the most important predictors being monthly cloud fraction, mean annual and monthly temperatures and elevation. Regression models for FAPAR (monthly images) gave an R-square of 90 % with most important predictors being total annual precipitation, monthly cloud fraction, CHELSA bioclimatic layers and month of the year, respectively. Further developments of PNV mapping could include using GBIF records to map global distribution of plant species at different taxonomic levels. This methodology could also be extended to dynamic modeling of PNV, so that future climate scenarios can be incorporated. Global maps of biomes, FAPAR and tree species at 1 km spatial resolution are available for download via <http://dx.doi.org/10.7910/DVN/QQHCHK>.

Submitted to PeerJ on 26th of March 2018

## INTRODUCTION

Potential Natural Vegetation (PNV) is the “*vegetation cover in equilibrium with climate, that would exist at a given location non-impacted by human activities*” (Levvasseur et al., 2012). It is a hypothetical vegetation state assuming natural (undisturbed) physical conditions, a reference status of vegetation assuming no degradation and/or no unusual ecological disturbances. PNV is especially useful for raising public awareness about land degradation and for estimating land potential (Herrick et al., 2013). For example, Omernik (1987) details PNV maps for USA; Bohn et al. (2007) provides maps for EU; Carnahan (1989) for Australia; Marinova et al. (2017) maps PNV for the Eastern Mediterranean–Black Sea–Caspian–Corridor; and maps of PNV for Latin America are available in Marchant et al. (2009). Regarding specific tree species, San-Miguel-Ayanz et al. (2016) provide habitat suitability maps for the main forest tree species in Europe, based on environmental variables, especially bioclimatic variables such as average temperature of the coldest month, precipitation of the driest month and similar. Potapov et al. (2011) have generated a global map of potential forest cover at 1 km resolution (publicly available from <http://globalforestwatch.org/map/>). Erb et al. (2017) produced a global map of potential biomass stocks by reversing the current managed land use systems to natural vegetation. Levvasseur et al. (2012) and Tian et al. (2016) predict global PNV classes using environmental covariates such as climatic

59 images and landform parameters. [Griscom et al. \(2017\)](#) have recently produced a global reforestation  
60 map at 1 km resolution.

61 A common limitation of prior maps is their coarse spatial resolution (about 25 km) limiting the use of  
62 these maps for operational planning (e.g. [Marchant et al. \(2009\)](#); [Levvasseur et al. \(2012\)](#) and [Tian et al.](#)  
63 [\(2016\)](#)). In addition, comparisons of multiple overlapping sources of PNV maps shows that they rarely  
64 agree with one another since they do not share the same mapping criteria and, traditionally, emphasize  
65 regionally-specific botanical groupings rather than functional classifications. Limitations of maps based  
66 on field surveys of PNV (e.g., [Bohn et al. \(2007\)](#)) are the assumptions about the controls on vegetation  
67 distribution applied to the extrapolation of a limited number of field surveys.

68 Here we provide an update of comparable global PNV maps produced by [Potapov et al. \(2011\)](#);  
69 [Levvasseur et al. \(2012\)](#); [Tian et al. \(2016\)](#) and [Erb et al. \(2017\)](#). We explore the possibility of increasing  
70 the mapping accuracy using up-to-date maps of climate, atmosphere dynamics, landform and lithology,  
71 and state-of-the-art machine learning methods. Our final aim is to produce PNV maps that are both more  
72 detailed, richer in information, based on objective reproducible methods; and potentially more usable  
73 for global modeling and awareness raising projects. We focus on improving the spatial detail, thematic  
74 accuracy and reproducibility of maps, at the cost of increasing the total computing load, but also consider  
75 automation of the prediction process so that the maps can be rapidly updated as the new ground data  
76 arrives. Our modeling follows three phases:

- 77 (a) model selection: we compare possible models of interest for PNV mapping and choose the optimal  
78 spatial prediction framework based on the cross-validation results,
- 79 (b) model assessment: we assess the uncertainty of predictions per vegetation class and try to determine  
80 objectively the limitations of the mapping products for wider uses, and
- 81 (c) prediction: we use the best performing models to produce spatial predictions, then visually assess  
82 maps and if necessary repeat steps a–c.

## 83 METHODS AND MATERIALS

### 84 Theory

85 PNV is the hypothetical vegetation cover that would be present if the vegetation were in equilibrium with  
86 environmental controls, including climatic factors and disturbance, and not subject to human management.  
87 When considering PNV, one needs to distinguish between potential “*natural*” and potential “*managed*”  
88 vegetation, and “*actual*” natural and “*actual*” managed vegetation. PNV also changes through time,  
89 therefore it can refer to the current state of environment or some past historic state (Fig. 1b). However,  
90 parts of the world that have not been subject to human disturbance/management can provide clearer  
91 information about the vegetation cover in historic times which can serve as a guide to PNV. A major  
92 limitation of modeling PNV is that we unfortunately do not have equally detailed information about  
93 the status of vegetation and environment across historic periods. For instance, about half of the Earth’s  
94 mature tropical forests have disappeared in the last 150 years and original habitats have reduced to 10 %  
95 ([Hansen et al., 2013](#)). Given that climates have changed and few areas are truly “*human impact free*”,

even undisturbed historic vegetation only represents the expression of PNV for a given set of climate conditions at a specific time.

Regardless of the hypothetical nature of PNV, the concept (both as a classification and as a regression type problem) is still a helpful yardstick against which land cover change can be quantitatively measured and land restoration designs could be planned. Indeed Erb et al. (2017) have estimated that almost half of the standing global vegetation biomass carbon stocks have been lost, almost equally due to land cover change (e.g. tree cover to cropland) and management effects within land cover types (e.g. croplands managed at lower biomass carbon stocks than tree covered areas). PNV maps can help quantify the differences (both deficit and surplus) in biomass stocks caused by the current land management system more objectively. For efforts aimed at land restoration, such information could also be a valuable input into the redesign of land management systems.

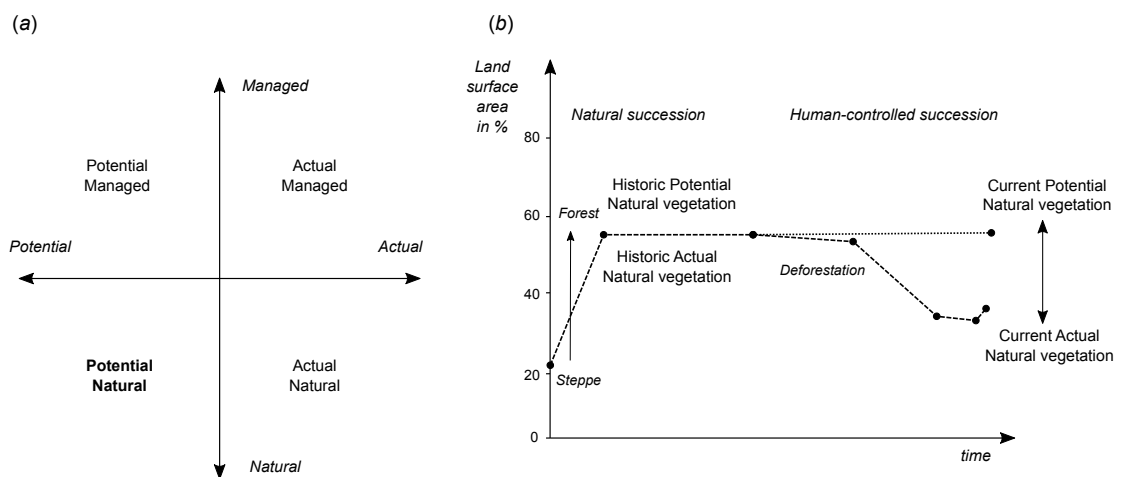


**Figure 1.** Schematic explanation of differences between (a) potential and actual natural/managed vegetation, and (b) current and historic vegetation. This paper focuses on providing estimates of Potential Natural Vegetation (PNV) using current state biophysical conditions.

Mapping PNV is a special case of species distribution modeling (Elith and Leathwick, 2009; Hijmans and Elith, 2018): at the core of PNV mapping is statistical modeling of relationship between species (or natural association of species or communities) and a list of predictors i.e. biotic and abiotic site factors (Elith and Leathwick, 2009). The difference between mapping actual distribution of species and mapping PNV is that PNV involves extrapolating the model to the whole land mask, assuming a hypothetical distribution under a specific set of undisturbed bioclimatic and/or biophysical conditions:

$$\Pr(Y) = f(\text{Relief, BioClimate, Lithology}) \quad (1)$$

where  $Y$  is the target variable, which could be vegetation types or plant species with finite number of states  $Y \in \{1, 2, \dots, k\}$  and/or vegetation properties. PNV mapping can be considered as a *classification-type* or *regression-type* problem depending on whether we map factors such as vegetation types or continuous vegetation properties such as biomass or leaf area index.

117 The primary assumptions we make when applying a PNV model to the training data are:

- 118 1. The ecological gradients captured in training data reflect only natural ecological gradients and  
119 not human controls such as land use systems, civil engineering constructions, or one-off major  
120 disturbance events such as volcanic eruptions, floods, or tsunamis.
- 121 2. Remote sensing data such NDVI reflect human-altered vegetation patterns and ought not be used as  
122 covariates in PNV mapping (Leong and Roderick, 2015).
- 123 3. The training data are representative of the study area, especially considering the feature space  
124 (ecological gradients) of the study area.

125 Assuming a log-linear relationship between ecological gradients and target variables, PNV classes  
126 can be modeled using a multinomial log-linear model:

$$f(k, i) = \beta_{0,k} + \beta_{1,k}x_{1,i} + \beta_{2,k}x_{2,i} + \dots + \beta_{M,k}x_{M,i} \quad (2)$$

127 where  $f(k, i)$  is the linear predictor function,  $\beta$  are the regression coefficients associated with the  $m$ th  
128 explanatory variable and the  $k$ th outcome. An efficient implementation of the multinomial logistic  
129 regression is the `multinom` function from the R package `nnet` (Venables and Ripley, 2002). The output of  
130 prediction produced using `multinom` are  $k$  probability maps (0–100 %) such that all predictions at each  
131 site sum up to 1:

$$\sum_{k=1}^K \Pr(Y_i = k) = 1 \quad (3)$$

132 In this paper, all predictions models are used in the “probability” mode i.e. to derive probability maps  
133 per class.

134 Note that a PNV spatial prediction model divides geographic space among all possible states given  
135 the training points. It is therefore necessary, for Eq.(1), that all possible states of  $Y$  are represented with  
136 training data so that the model can be applied over the whole spatial domain of interest. If not all of the  
137 states are known, then the space will be artificially filled-in with classes occupying similar ecological  
138 niches and which can lead to prediction bias. In other words, similar to species distribution modeling of  
139 individual species, both presence and absence data play an equally important role for model calibration  
140 (Elith and Leathwick, 2009).

#### 141 **Input data: training points**

142 We consider three ground-truth data sets for model calibration:

- 143 1. an expanded version of the BIOME 6000 DB data set representing site-based reconstructions from  
144 surface pollen samples of major vegetation types or biomes ([http://dx.doi.org/10.17864/](http://dx.doi.org/10.17864/1947.99)  
145 [1947.99](http://dx.doi.org/10.17864/1947.99)),



2. EU Forest (Mauri et al., 2017) and GBIF (Global Biodiversity Information Facilities) occurrence records of the 76 main forest tree taxa in Europe (<http://dx.doi.org/10.15468/dl.fhucwx>),

3. Long-term Fraction of Absorbed Photosynthetically Active Radiation (FAPAR) monthly images derived using a time-series of Copernicus Global Land products (<https://land.copernicus.eu>),

BIOME 6000 and EU Forest and GBIF occurrences are point data sets, while FAPAR are remote sensing images at relatively fine spatial resolution (250 m), from which we sample large number of values (ca 100,000) using random sampling after masking for areas of natural vegetation.

### BIOME 6000

The BIOME 6000 data set (<http://dx.doi.org/10.17864/1947.99>) includes vegetation reconstructions from modern pollen samples, preserved in lake and bog sediments and from moss polsters, soil and other surface deposits. The use of pollen data to reconstruct PNV relies on the fact that although modern pollen samples may contain markers of land use, the predominant pollen types found in any one sample are those of the regional vegetation within a radius on the order of 10–30 km around the sampling site. Even if forests have fragmented, these fragments continue to produce and disperse pollen grains, and the composition of the pollen assemblage provides information on tree taxa that are still present.

The BIOME 6000 data set is an amalgamation of multiple data sets. BIOME 6000 initially produced maps for individual regions: Europe, Africa and the Arabian Peninsula, the Former Soviet Union and Mongolia and China. Additional regions were subsequently added including Beringia, western North America, Canada and the eastern United States and Japan, and the data for northern Eurasia, China and southern Europe and Africa were also updated. These regional compilations were summarized in Prentice and Jolly (2000). Subsequent regional updates include China (Harrison et al., 2001), the circum-Artic region (Bigelow et al., 2003), Australia (Pickett et al., 2004) and South America (Marchant et al., 2009). Additionally, we have also combined these data with pollen-based vegetation reconstructions from the Eastern Mediterranean-Black Sea-Caspian Corridor (EMBSecBIO) region (Marinova et al., 2017) available from <http://dx.doi.org/10.17864/1947.109>, to produce a more complete and up-to-date compilation of the BIOME 6000.

Some sites in the BIOME 6000 data set have multiple reconstructions based on multiple nearby modern pollen samples (up to 30), which provides a useful measure of the reconstruction uncertainty, but could lead to modeling bias because the number of modern samples varies between sites. To reduce these unwanted effects, we use only the most frequently reconstructed biome at each site and for the sites with two equally common reconstructions (ca. 900) we use both observations.

The number of biomes differentiated varies from region to region, and some biomes were only reconstructed in specific regions where they are particularly characteristic, although they may occur elsewhere. Furthermore, some biomes that can be recognized on the modern landscape were never reconstructed in the BIOME 6000 data set (e.g. cushion forb tundra) — either because of the sample distribution or because the characteristic plant-functional types were also spread amongst other biomes. Simplified or “megabiome” classifications (e.g. Harrison and Bartlein (2012)) involve a substantial loss

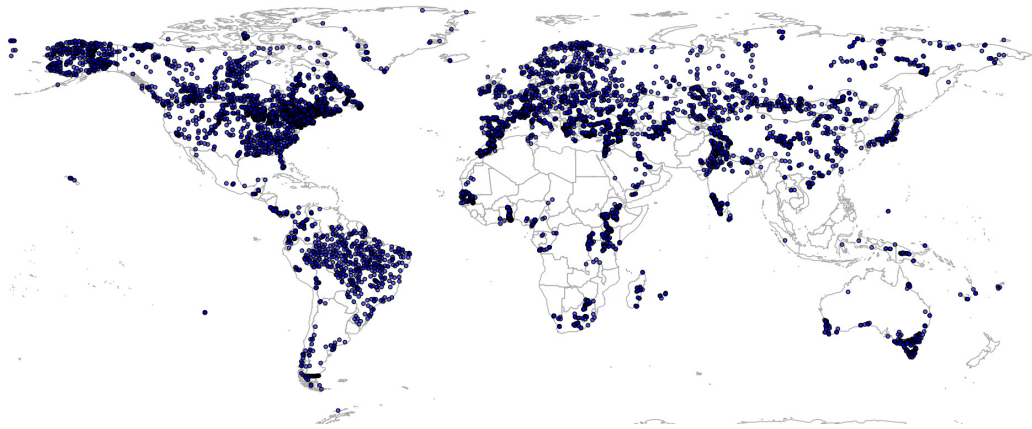


**Figure 2.** Spatial distribution of BIOME 6000 training points. A total of 8057 unique locations are shown on the map.

of information. We have therefore created a new standardization of the classification scheme (see further Table 1; the final scheme has 20 globally applicable and distinctive biomes) which preserve the maximum number of distinct biomes that were reconstructed as present in multiple regions.

There are relatively few data vegetation reconstructions for tropical South America, which could lead to extrapolation problems and omission of important PNV classes in Latin America, but also potentially in tropical parts of Africa and Asia. To reduce under-representation of tropics, we have added 350 randomly simulated points based on the RADAM Brazil natural vegetation polygon map at high spatial detail (Radam Vegetação SIRGAS map) (Veloso et al., 1992) obtained from <ftp://geofftp.ibge.gov.br/>. Before generating the pseudo-observations for Brazil, we have translated SIRGAS map legends to match the BIOME 6000 classes. This translation is also available via the project's github repository. This gave a total of 8057 unique individual locations represented in the combined data set i.e. a total of 8959 training observations (Fig. 2).

We have mapped the distribution of biomes for all land pixels, with the exception of water bodies, barren land and permanent ice areas. Barren land and permanent ice areas were masked out using the ESA's global land cover maps for the period 2000–2015 (<https://www.esa-landcover-cci.org>) and the long-term FAPAR images, both available at relatively fine resolution of 300 m. We only mask out pixels that are permanent ice/barren ground and have a FAPAR = 0 throughout the period 2000–2015.

#### European Forest Tree occurrence records

For mapping PNV distribution of forest tree taxa (note: most of these are individual species, but some are only recognised at sub-genus or genus level) in Europe we have merged two point data sets: EU Forest (Mauri et al., 2017) (588,983 records covering 242 species) and GBIF occurrence records of the main forest tree taxa in Europe. The GBIF Occurrence data was downloaded on 23rd January 2017 (<http://dx.doi.org/10.15468/dl.fhucwx>). We focus on modeling just the 76 forest tree taxa indicated in the European Atlas of Forest Tree Species (San-Miguel-Ayanz et al., 2016).

Global GBIF occurrence data can be obtained by using the `rgbif` package, in which case the only important parameter is the `taxonKey` (e.g. "*Betula spp.*" corresponds to GBIF taxon key 2875008). After

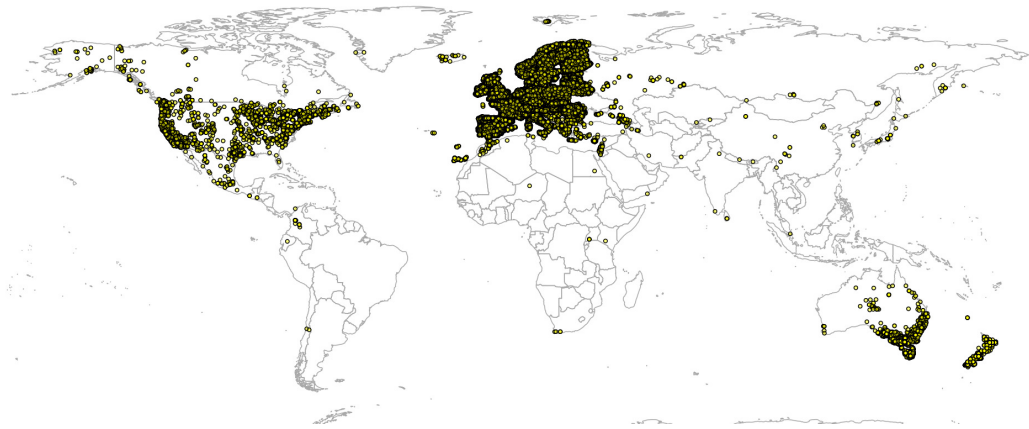


**Figure 3.** Merge of EU Forest (Mauri et al., 2017) and GBIF occurrence records used to build models to predict PNV for the 76 forest tree taxa. Total of 1,546,435 shown on the map.

the bulk data download (which gives about 4 million occurrences), we imported all points and then subset occurrences based on the list of taxon keys and coordinate uncertainty ( $<2$  km positional error). This gave a total of 1,546,435 training points from which about 2/3 are GBIF points (Fig. 3). We assume in further analysis that the EU Forest point locations and representativeness are more trustworthy, hence we assign  $4\times$  higher weights to these points than to the GBIF points.

Certain forest tree species (*Chamaecyparis lawsoniana*, *Eucalyptus globulus* and *Pseudotsuga menziesii*), that are shown in the European Atlas of Forest Tree Species are introduced i.e. planted and do not generally propagate naturally. Hence, they were removed from the list of target forest tree species. We retained, however, three species (*Ailanthus altissima*, *Picea sitchensis* and *Robinia pseudoacacia*) that are not native but are extensively naturalized. The total number of target forest tree taxa was 73.

We built predictive models for European forest tree taxa using information on their global distribution, but only generate predictions for Europe. In other words, we use a global compilation for model training to increase the precision of the definition of the ecological niche of each taxon, but then predict only for Europe as the selection of taxa is based on the European Atlas of Forest Tree Species (San-Miguel-Ayanz et al., 2016).

## FAPAR

Fraction of Absorbed Photosynthetically Active Radiation (FAPAR) monthly images for 2014–2017 were obtained from <https://land.copernicus.eu>. From a total of 142 images downloaded from <https://land.copernicus.eu> we derived minimum, median and maximum value of FAPAR per month (12) using the 95 % probability interval using the data.table package (<http://r-datatable.com>). For regression modeling we only show results of predictions of median values of FAPAR; predictions of minimum and maximum FAPAR can be obtained from the data repository.

We model median and upper 95 % FAPAR values as a function of the same covariate layers used in all three case studies. For model training we use ca. 30,000 randomly sampled points (Simple Random Sampling) exclusively from protected area as shown in the World Database on Protected Areas (WDPA) data set (<http://protectedplanet.net>) and the Intact Forest Landscapes (IFL) data set for 2000 and

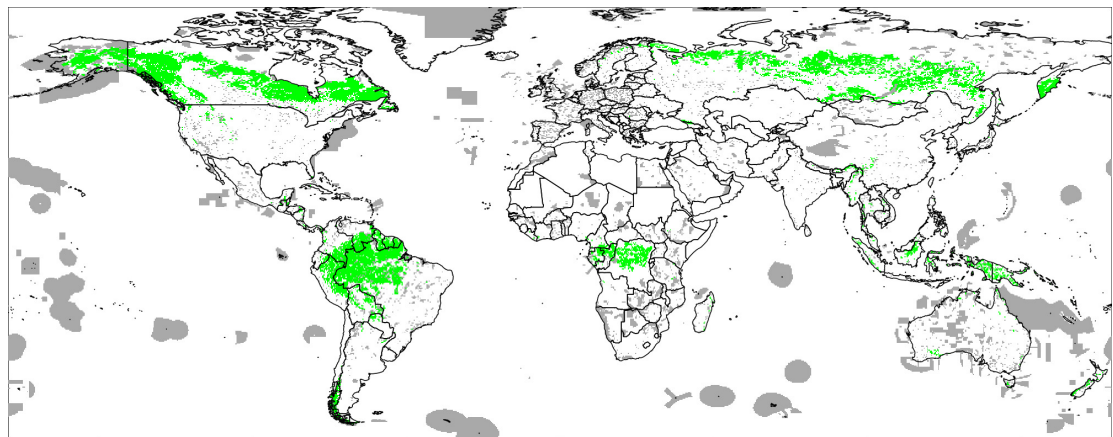


**Figure 4.** World's Protected Areas (dark gray) based on <http://protectedplanet.net> and Intact Forest Landscapes for year 2000 (green) based on <http://intactforests.org>. These maps were used to randomly select some 30,000 training points to predict potential FAPAR under PNV.

2013 (Potapov et al., 2008) Fig. 4). We use about  $3\times$  more training points from the IFL 2013 areas than from the WDPA and IFL 2000 masks to emphasize ecological conditions of intact vegetation.

The prediction model for FAPAR under PNV is in the form of:

$$R> \text{FAPAR} \sim c_m + X_{1m} + X_{2m} + X_3 + \dots + X_p$$

where  $X_{1m}$  is the covariate with monthly values (for example precipitation, day-time and night-time temperatures etc),  $X_3$  is the environmental covariates that does not vary through year (e.g. lithology or DEM derivatives), and  $c_m$  is the cosine of the month number:

$$c_m = \cos(\mu/12 \cdot 2 \cdot \pi) \quad (4)$$

where  $\mu$  is the month number 1–12. The total number of training observations used to build models is in fact 180,483 (each training site is represented up to 12 times).

For PNV FAPAR mapping we have masked out all water bodies including lakes and rivers, following the ESA's global land cover maps for the period 2000–2015 (<https://www.esa-landcover-cci.org>) and permanent ice/barren ground.

#### Input data: environmental covariates

For modeling purposes, we use a stack of 160 spatially explicit co-variate data layers that represent ecological gradients essential for growth and survival of plants:

- DEM derivatives quantifying various landscape metrics and hydrological processes: slope, curvature, topographic index, topographic openness, valley depth and multi-resolution valley bottom index; all derived using the SAGA GIS (Conrad et al., 2015);
- Mean, minimum and maximum monthly temperatures derived as a mean between WorldClim v2 (<http://worldclim.org/version2>) and CHELSA climate (Karger et al., 2017).

- Mean monthly precipitation images derived as a weighted average between the WorldClim v2, CHELSA climate and Global Precipitation Measurement Integrated Multi-satellite Retrievals for GPM (IMERG) rainfall product.
- CHELSA Bioclimatic layers downloaded from <http://chelsa-climate.org/>, including: annual mean temperature, mean diurnal temperature range, isothermality (day-to-night temperature oscillations relative to the summer-to-winter oscillations), temperature seasonality (standard deviation of monthly temperature averages), maximum temperature of warmest month, minimum temperature of coldest month, temperature annual range, mean temperature of warmest quarter, mean temperature of coldest quarter, annual precipitation amount, precipitation of wettest month, precipitation of driest month, precipitation of wettest quarter, precipitation of driest quarter (Karger et al., 2017);
- European Space Agency's CCI-LC snow probability monthly averages based on MODIS snow products MOD10A2 downloaded from <http://maps.elie.ucl.ac.be/CCI/viewer/index.php>;
- USGS Global Ecophysiology landform classification and lithological map at 250 m resolution obtained from <http://rmgsc.cr.usgs.gov/outgoing/ecosystems/Global/> and based on Global Lithological Map (GLiM) (Hartmann and Moosdorf, 2012);
- MODIS Cloud fraction monthly images obtained from <http://www.earthenv.org/cloud> (Wilson and Jetz, 2016);
- Global Water Table Depth in meters based on Fan et al. (2013);
- NASA's monthly MODIS Precipitable Water Vapor images (MYDAL2\_M\_SKY\_WV data set at <http://neo.sci.gsfc.nasa.gov>);
- Potential wetlands GIEMS map (Fluet-Chouinard et al., 2015);
- Global Surface Water dynamics images: occurrence probability, surface water change, and water maximum extent; downloaded from <https://global-surface-water.appspot.com/download> (Pekel et al., 2016);
- Density of earthquakes based on the USGS Earthquake Archives (<http://earthquake.usgs.gov/earthquakes/>);

Some CHELSA bioclimatic layers contained too many missing pixels or artifacts (e.g. mean temperature of wettest quarter, mean temperature of driest quarter, precipitation seasonality, precipitation of warmest quarter and precipitation of coldest quarter) and were hence not used for further modeling to avoid propagating those artifacts to final predictions.

All original layers have been resampled to the same grid at spatial resolution of 1/120 decimal degrees (about 1 km) covering latitudes between -62.0 and 87.37. We do not map Antarctica as this continent is dominantly covered with permanent ice and there are no training points. We limit all analysis to 1 km i.e. 1/120 degrees in geographical coordinates, to avoid too high computational load, even though many of environmental covariates are also available at finer resolutions.

We use the same stack of covariates for mapping global distribution of biomes, FAPAR and forest tree species in Europe, to be able to compare model performance and investigate whether the most important



294 covariates differ between the three case studies.

## 295 **Machine Learning Algorithms (MLA) examined**

296 We examine predictive performance of the following MLA's:

- 297 • Neural networks (Venables and Ripley, 2002),
- 298 • Random forest (Breiman, 2001; Cutler et al., 2007; Biau and Scornet, 2016; Hengl et al., 2018),
- 299 • Generalized Boosted Regression Models (Friedman, 2002),
- 300 • K-nearest neighbors (Venables and Ripley, 2002),

301 Neural networks are available from several packages in R. Here we use the nnet package (Ripley and  
302 Venables, 2017) also described in Venables and Ripley (2002). Random forest is efficiently implemented in  
303 the ranger package (Wright and Ziegler, 2016) and can be used to process large data sets. Generalized  
304 Boosted Regression Models are available via the gbm package (Ridgeway, 2017). The K-nearest  
305 Neighbour Regression is available via the class package i.e. the knn function (Venables and Ripley,  
306 2002). Of these four algorithms, the K-nearest neighbors is computationally least intensive and results  
307 in relatively simple models, while random forest is computationally most intensive and results in large  
308 models. However, a limitation of the K-nearest neighbors approach is that it does not handle high  
309 dimensional data in comparison to random forest or neural nets.

310 We also test using the same packages to fit models for regression-type problems (e.g. modeling  
311 of FAPAR), with the exception of the class package i.e. the knn function which can only be used for  
312 classification problems. For modeling FAPAR we used instead also the Cubist approach, available via  
313 the Cubist package (Kuhn et al., 2014), and the Extreme Gradient Boosting approach available via the  
314 xgboost package (Chen and Guestrin, 2016).

315 The caret package has many more MLA of interest for classification and regression problems than  
316 presented here, but many are not all optimized for large data sets and hence also not applicable for large  
317 data sets ( $\gg$  1000 observations with  $\gg$  100 covariates).

## 318 **Model selection**

319 For model fitting and model selection we use the caret package implementation for automated evaluation  
320 of models. When comparing performance of the models we look at classification accuracy based on  
321 cross-validation with refitting implemented in the caret package via the setting (Kuhn, 2008; Kuhn and  
322 Johnson, 2013):

```
R> ctrl <- trainControl(method="repeatedcv", number=5, repeats=2)
```

323 which translates as: models are refit 5 times using 80 % of the data and that predictions derived from the  
324 fitted models are compared with the remaining observations; this process is then repeated two times to  
325 produce stable results. The reported accuracy is the map accuracy (0–100 %) and/or Root Mean Square  
326 Error (RMSE) derived using all merged cross-validations (Kuhn, 2008; Kuhn and Johnson, 2013). Since  
327 most of data sets are fairly large and model fitting can take hours, even in a High Performance Computing  
328 environment, we limit the number of repetitions to 2.

For FAPAR (regression modeling) and selection of the final prediction model we use the same repeated cross-validation as implemented via the caret package. This is in principle similar to evaluation of the classification accuracy, except the comparison criterion is RMSE.

All analyses were run on a High Performance Computing Amazon ec2 server with 64 cores and 256 GiB RAM. Total computing time to produce all outputs is about 12 hours of optimized computing (or about 600 CPU hours). 1 km data can be processed with 2 degree tiles, which usually leads to some 5000 tiles to represent the land mask. All processing steps and preparation of input and output maps are fully documented at <https://github.com/envirometrix/PNVmaps>. All output maps are available for download via <http://dx.doi.org/10.7910/DVN/QQHC1K> under the Open Database License (ODbL).

### Performance of classification algorithms

For biomes and tree species we use the map purity (0–100 %) and kappa metrics for the dominant (hard) classes at cross-validation points as the key measure of predictive performance (Kuhn and Johnson, 2013). For each class we also provide predicted probabilities, which can be used to model transition zones and correlation between classes. For the predicted probabilities of class occurrences (0–1) we derived the True Positive Rate (TPR) and the Area Under the receiver operating characteristic Curve (AUC) as implemented in the ROCR package (Sing et al., 2005, 2016). TPR values range from 0 to 1 where 1 indicates a perfect match to the class positives in ground data and TPR values < 0.5 can be considered poor. Values of AUC close to 1 show high prediction performance, while values around 0.5 and below are considered poor. TPR and AUC provide probably a more informative measure of the mapping accuracy than overall mapping accuracy / kappa, as they also allow detection of problematic classes.

We also use Scaled Shannon Entropy Index, which can be derived using the per-class probability maps (Shannon, 1949; Borda, 2011):

$$El_s(x) = - \sum_{i=1}^b P_i(x) \cdot \log_b P_i(x) = \frac{- \sum_{i=1}^b P_i(x) \cdot \log P_i(x)}{-b \cdot b^{-1} \cdot \log b^{-1}} \quad (5)$$

where  $b$  is the total number of possible classes and  $P$  is probability of class  $i$ . The Scaled Shannon Entropy Index ( $El_s$ ) is in the range from 0–1, where 0 indicates a perfect classification and 1 (or 100 %) indicates maximum confusion. Scaled Shannon Entropy Index should not be confused with classification accuracy assessment:  $El_s < 60$  % already indicates relatively low confusion between classes i.e. high accuracy, while mapping error of 60 % would still be considered a relatively poor classification accuracy result.

For the biomes data set, where spatial clustering of points is significant, we also use repeated spatial cross-validation as implemented in the mlr package (Bischl et al., 2016):

```
R> learner.rf = makeLearner("classif.ranger", predict.type = "prob")
R> resampling = makeResampleDesc("RepCV", fold = 5, reps = 5)
```

It has been shown that spatial autocorrelation in data and serious spatial clustering in training points can lead to somewhat biased estimate of the actual accuracy (Brenning, 2012). Solution to this problem is to apply spatial partitioning so that possible bias due to spatial proximity is minimized.

We also compare results of modeling potential distribution of tree species in Europe with the habitat type maps of Europe produced independently by San-Miguel-Ayanz et al. (2016) and Brus et al. (2012). This comparison is visually based only.

#### Performance of regression algorithms

For testing spatial predictability of FAPAR we use the root mean squared error (RMSE) and mean error (ME):

$$\text{RMSE} = \sqrt{\frac{\sum_{j=1}^m [\hat{y}(\mathbf{s}_j) - y(\mathbf{s}_j)]^2}{n}}$$

$$\text{ME} = \frac{\sum_{j=1}^m [\hat{y}(\mathbf{s}_j) - y(\mathbf{s}_j)]}{n}$$

where  $\hat{y}(\mathbf{s}_j)$  is the predicted value of  $y$  at the cross-validation location, and  $m$  is total number of cross-validation points. We also report amount of variation explained by the model ( $R^2$ ) derived as:

$$R^2 = \left[ 1 - \frac{SSE}{SST} \right] \times 100\% \quad (6)$$

where  $SSE$  is the sum of squared errors at cross-validation points and  $SST$  is the total sum of squares. A coefficient of determination close to 1 indicates a perfect model.

## RESULTS

### Global maps of biomes

Results show that a relatively accurate model of PNV can be produced from the BIOME 6000 data set using the existing stack of covariates at 1 km spatial resolution. Results of cross-validation show that random forest (RF) model is the best performing method and distinctively better than other approaches (Fig. 5). The choice of the random forest `mtry` parameter has little impact on overall accuracy, most likely because there is a high overlap in covariate maps so that even with smaller `mtry` bagging the performance is relatively similar. The best prediction accuracy from the four methods used for mapping global biomes is about 68 %. The predicted biome classes are available in Fig. 6.

The most important covariates for the random forest model are: total annual precipitation, monthly temperatures, CHELSA bioclimatic layers, atmospheric water vapor images and monthly precipitation. Landform parameters and lithology are not amongst the top 20 most important predictors. The decline in variable importance is, however, gradual — even lower ranked covariates might still affect the accuracy of predictions.

The detailed cross-validation results show that the only difficult classes to predict is prostrate dwarf shrub tundra (Table 1). The TPR value for most class probabilities ranges from 0.83 to 0.94 indicating relatively high match with ground data. The Scaled Shannon Entropy Index map (Fig. 7) shows that the zones of highest confusion between classes can be found in Afghanistan, Nepal, mountainous parts of the USA and Mexico, parts of Angola and Zambia. The map of the SSEI is comparable to the confusion map



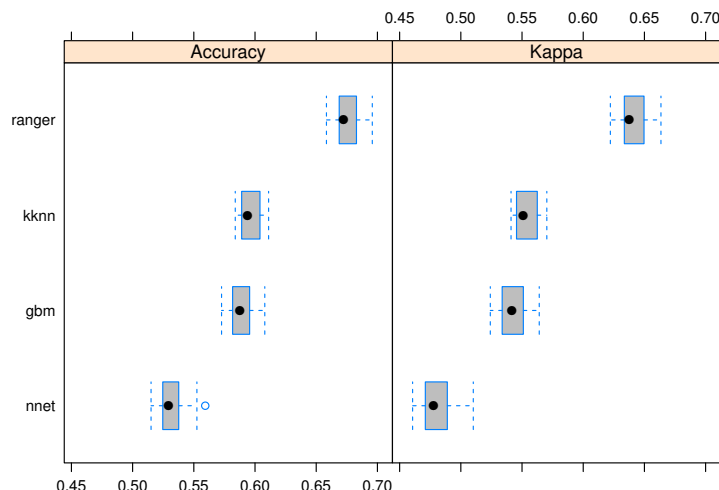


**Figure 5.** Predictive performance of the target machine learning algorithms for mapping global distribution of biomes ( $N = 8653$ ; spatial distribution of training points is available in Fig. 2). ranger = random forest, kkn = K-nearest neighbors, gbm = Generalized Boosted Regression Models, nnet = Neural networks.

**Table 1.** Summary results of cross-validation for mapping global distribution of biomes (20 classes). Classification accuracy for predicted class probabilities based on 5-fold cross-validation with refitting. ME = “Mean Error”, TPR = “True Positive Rate”, AUC = “Area Under Curve”, N = “Number of occurrences”.

Biome class	ME	TPR	AUC	N
cold deciduous forest	-0.01	0.89	0.96	201
cold evergreen needleleaf forest	0.01	0.87	0.98	892
cool evergreen needleleaf forest	-0.07	0.87	0.93	201
cool mixed forest	0.01	0.86	0.97	1549
cool temperate rainforest	0.01	0.92	0.99	95
desert	0.00	0.89	0.96	330
erect dwarf shrub tundra	-0.01	0.89	0.98	145
graminoid and forb tundra	-0.03	0.83	0.91	128
low and high shrub tundra	-0.01	0.88	0.98	393
prostrate dwarf shrub tundra	-0.02	<b>0.54</b>	0.90	11
steppe	0.01	0.87	0.94	889
temperate deciduous broadleaf forest	-0.01	0.84	0.94	961
temperate evergreen needleleaf open woodland	0.01	0.92	0.97	307
temperate sclerophyll woodland and shrubland	0.00	0.94	0.99	154
tropical deciduous broadleaf forest and woodland	0.01	0.86	0.97	215
tropical evergreen broadleaf forest	0.00	0.87	0.99	333
tropical savanna	0.01	0.89	0.99	291
tropical semi evergreen broadleaf forest	-0.05	0.87	0.98	160
warm temperate evergreen and mixed forest	0.01	0.85	0.96	985
xerophytic woods scrub	-0.02	0.88	0.95	388

390 produced by [Levvasseur et al. \(2012\)](#), except in our case the Rocky Mountains in USA and mountains  
391 chains in South America show somewhat higher confusion. Many of the areas with high confusion index  
392 happen because the prediction model has problems distinguishing between closely-related biomes such as

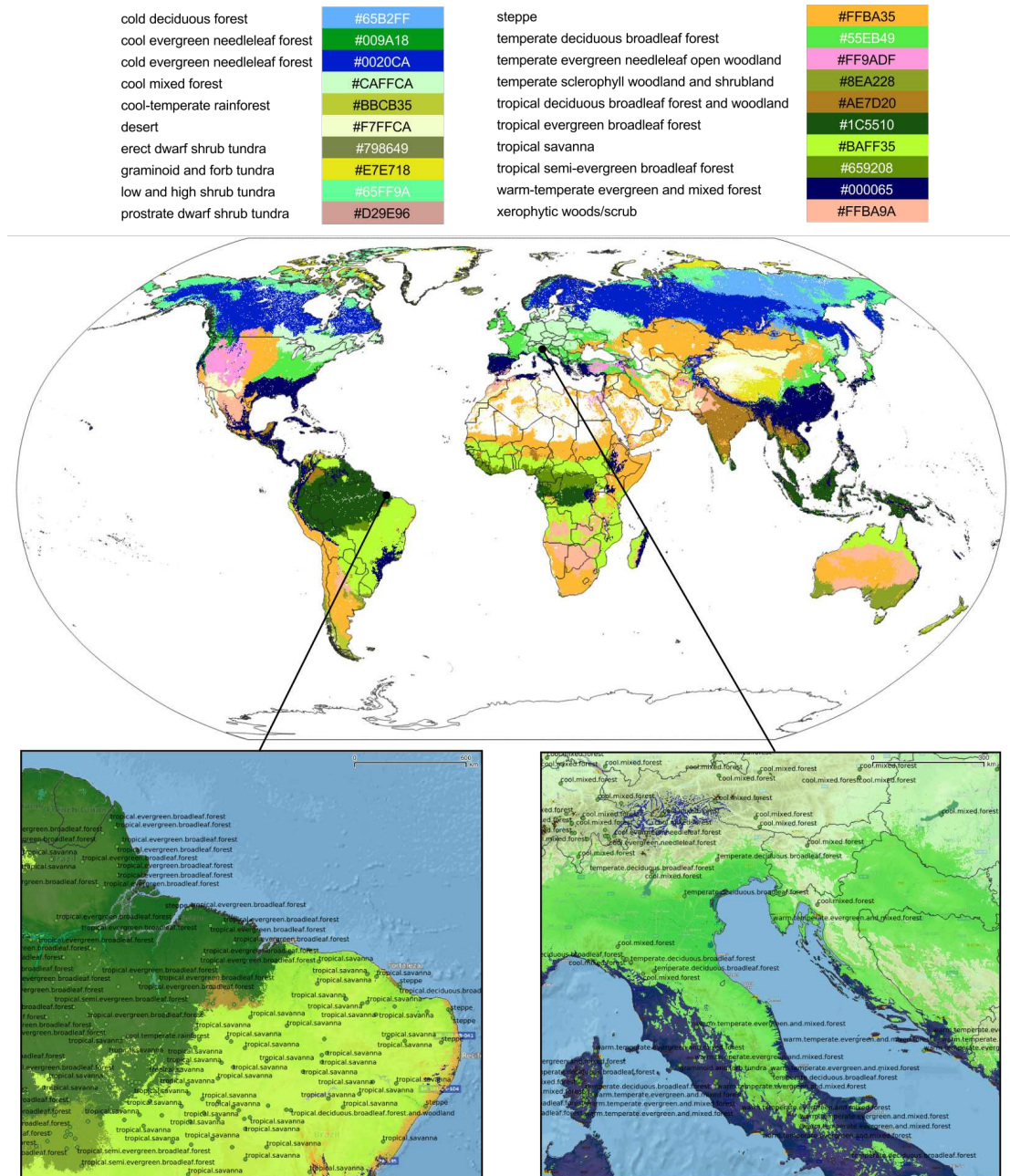


**Figure 6.** Predicted PNV distribution for global biomes with a zoom in on areas in Brazil and Europe. Labels indicates training points from the BIOME 6000 data set (Fig. 2).

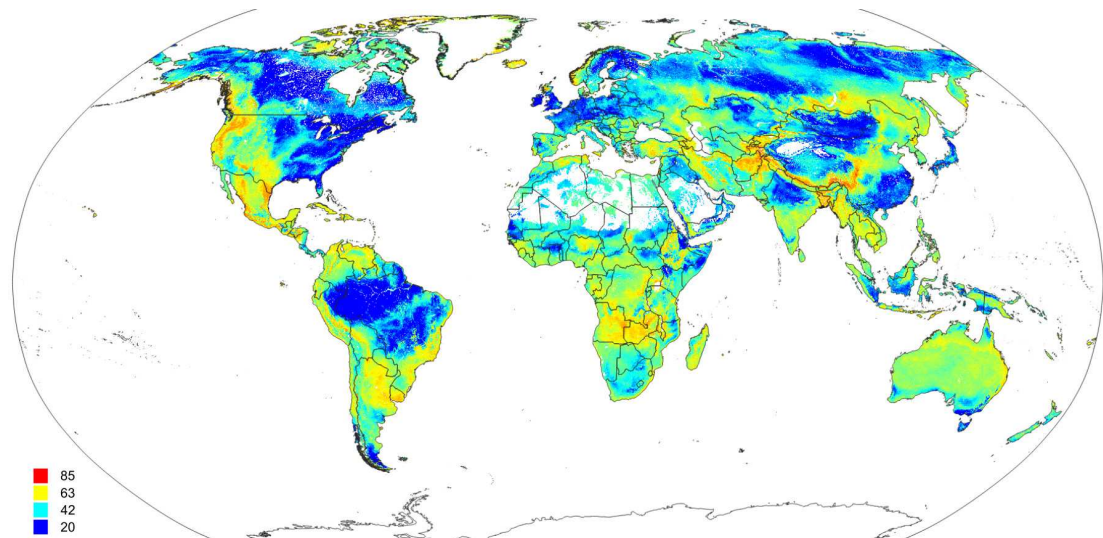


**Figure 7.** Scaled Shannon Entropy Index (SSEI) derived using predicted probabilities for 20 biomes (classes) based on Eq.(5). High values of SSEI (red color) indicate high confusion between classes.

the “cold evergreen needleleaf forest” and “cool evergreen needleleaf forest” (e.g. Scotland).

Results of the spatial Cross-Validation, as implemented in the mlr package (Bischl et al., 2016), further indicate that the spatial clustering of points does have a large effect on the mapping accuracy: spatial CV drops to 0.33 and weighted kappa to 0.45. This likely happens due to high spatial clustering of the biome points, but obviously biomes are also spatially highly autocorrelated.

### European forest tree species

The results of 5-fold cross validation with re-fitting at each fold, confirms that random forest is also the best prediction method for the forest taxa data set (Fig. 8). The overall mapping accuracy is significantly lower than for biomes, but this reduction in accuracy is to be expected as many of these taxa occur in communities, resulting in natural overlap of forest tree taxa distribution. The mapping accuracy of individual taxa, however, can be relatively high with TPR values of between 0.16–0.90 and an average value of around 0.69 (Table 2). The final maps (Fig. 9) show a relatively good match with ground data, meaning that with the exception of some species of rarer occurrence (*Picea omorika*, *Cupressus sempervirens*, *Prunus mahaleb*), the species probability distribution maps are relatively accurate.

**Table 2.** Results of cross-validation for the forest tree taxa (San-Miguel-Ayanz et al., 2016).

Classification accuracy for predicted class probabilities based on 5-fold cross-validation. ME = “Mean Error”, TPR = “True Positive Rate”, AUC = “Area Under Curve”, N = “Number of occurrences”. Taxa with less than < 50 observations were omitted from analysis.

Species name	GBIF taxon ID	ME	TPR	AUC	N
<i>Abies alba</i>	2685484	-0.01	0.77	0.92	16,150
<i>Acer campestre</i>	3189863	-0.01	0.65	0.83	19,819
<i>Acer platanoides</i>	3189846	-0.02	0.68	0.82	30,801
<i>Acer pseudoplatanus</i>	3189870	-0.01	0.69	0.79	65,039
<i>Aesculus hippocastanum</i>	3189815	-0.01	0.59	0.85	8,088
<i>Ailanthus altissima</i>	3190653	0.04	0.69	0.92	1,576
<i>Alnus cordata</i>	2876607	0.05	0.73	0.95	904

Continued on next page

Table 2 – Continued from previous page

Species name	GBIF taxon ID	ME	TPR	AUC	N
Alnus glutinosa	2876213	0.00	0.71	0.77	91,292
Alnus incana	2876388	-0.03	0.76	0.95	6,873
Betula spp.	2875008	-0.03	0.63	0.83	7,313
Carpinus betulus	2875818	0.00	0.75	0.89	22,765
Carpinus orientalis	2875780	0.07	<b>0.21</b>	0.92	284
Castanea sativa	5333294	0.00	0.74	0.91	13,049
Celtis australis	2984492	-0.01	0.54	0.92	594
Cornus mas	3082263	0.03	0.51	0.90	827
Cornus sanguinea	3082234	-0.03	0.59	0.82	8,837
Corylus avellana	2875979	-0.02	0.67	0.76	48,140
Cupressus sempervirens	2684030	-0.04	<b>0.21</b>	0.70	284
Euonymus europaeus	3169131	-0.02	0.61	0.83	12,119
Fagus sylvatica	2882316	0.00	0.73	0.81	89,044
Frangula alnus	3039454	-0.02	0.71	0.86	26,873
Fraxinus angustifolia	7325877	-0.05	0.63	0.94	1,757
Fraxinus excelsior	3172358	0.00	0.67	0.74	91,111
Fraxinus ornus	3172347	0.02	0.86	0.99	2,765
Ilex aquifolium	5414222	-0.01	0.66	0.82	26,873
Juglans regia	3054368	-0.03	0.60	0.89	3,643
Juniperus communis	2684709	-0.03	0.71	0.86	21,189
Juniperus oxycedrus	2684451	-0.07	0.71	0.97	1,705
Juniperus phoenicea	2684640	-0.07	0.74	0.98	1,137
Juniperus thurifera	2684528	-0.03	0.87	0.99	1,886
Larix decidua	2686212	-0.01	0.71	0.89	15,581
Olea europaea	5415040	0.00	0.90	0.99	7,080
Ostrya carpinifolia	5332305	0.06	0.90	0.99	1,809
Picea abies	5284884	0.02	0.76	0.86	122,713
Picea sitchensis	5284827	0.05	0.80	0.96	13,023
Pinus cembra	5285134	-0.01	0.77	0.96	853
Pinus halepensis and Pinus brutia	5285604	0.03	0.86	0.99	16,951
Pinus mugo	5285385	0.00	0.85	0.98	6,667
Pinus nigra	5284809	0.01	0.79	0.93	13,540
Pinus pinaster	5285565	0.01	0.86	0.98	17,080
Pinus pinea	5285165	-0.04	0.85	0.99	4,910
Pinus sylvestris	5285637	0.02	0.78	0.85	153,928
Populus alba	3040233	-0.01	0.54	0.86	4,522
Populus nigra	3040227	-0.01	0.65	0.89	5,478
Populus tremula	3040249	-0.02	0.66	0.74	44,057
Prunus avium	3020791	-0.01	0.63	0.77	25,711
Prunus cerasifera	3021730	0.00	0.73	0.94	3,928
Prunus mahaleb	3022789	-0.01	<b>0.31</b>	0.75	517
Prunus padus	3021037	-0.03	0.63	0.78	21,705
Prunus spinosa	3023221	-0.01	0.69	0.81	31,783
Quercus cerris	2880580	0.00	0.80	0.97	4,109
Quercus ilex	2879098	0.02	0.85	0.99	22,972
Quercus pubescens	2881283	0.01	0.86	0.98	9,096
Quercus pyrenaica	2878826	0.00	0.88	0.99	6,253
Quercus robur and Quercus petraea	2878688	0.01	0.69	0.76	141,938
Quercus suber	2879411	-0.04	0.86	0.99	5,504
Robinia pseudoacacia	5352251	0.01	0.71	0.90	13,411
Salix alba	5372513	0.02	0.72	0.90	11,938
Salix caprea	5372952	-0.03	0.68	0.78	40,879
Sambucus nigra	2888728	0.00	0.70	0.81	44,961
Sorbus aria	3012680	-0.01	0.59	0.87	5,426
Sorbus aucuparia	3012167	-0.01	0.70	0.76	86,977
Sorbus domestica	3013206	-0.04	<b>0.48</b>	0.87	801
Sorbus torminalis	3012567	-0.03	0.62	0.92	2,558
Taxus baccata	5284517	-0.02	0.58	0.82	8,062
Tilia spp.	3152041	-0.02	0.50	0.82	4,393
Ulmus spp.	2984510	-0.03	0.64	0.92	5,426
Tilia spp.	3152041	0.00	0.58	0.85	4,522
Ulmus spp.	2984510	-0.02	0.69	0.91	5,375



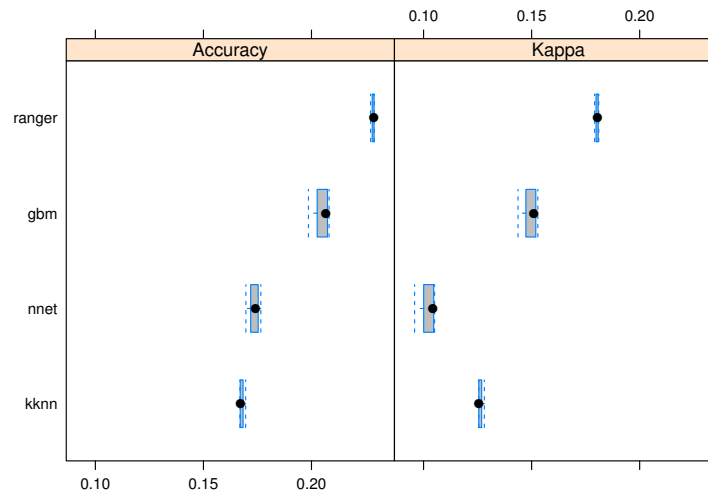


**Figure 8.** Predictive performance of the target machine learning algorithms for mapping forest tree species ( $N = 1.5$  million distribution of training points is available in Fig. 3). ranger = random forest, gbm = Generalized Boosted Regression Models, nnet = Neural networks, kkn = K-nearest neighbors.

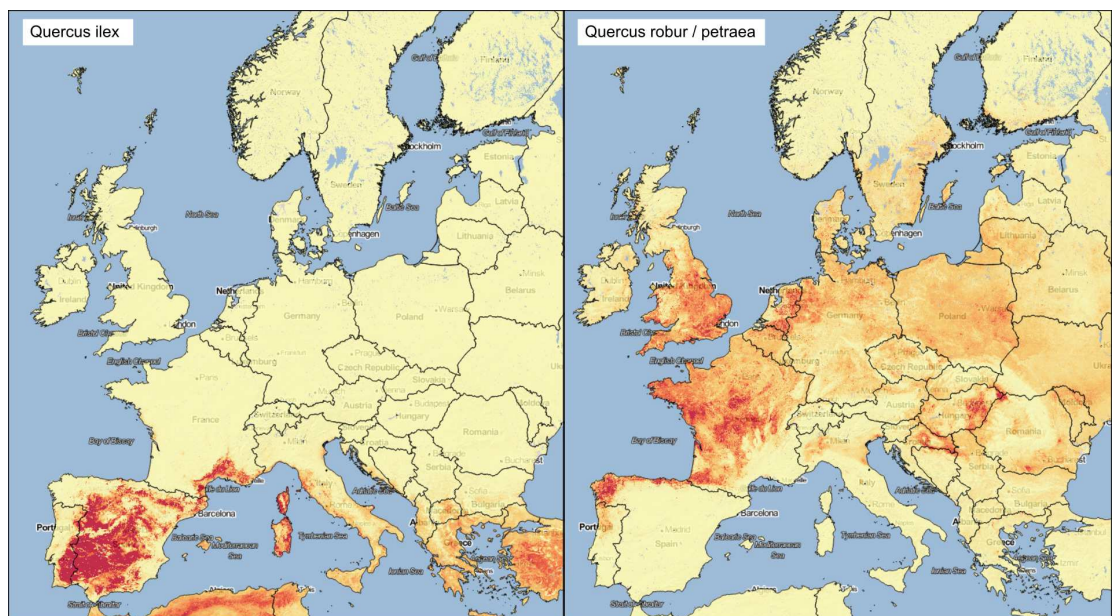


**Figure 9.** Examples of predicted PNV distributions (probabilities) for European forest tree species.

407

408 The most important predictors in the random forest model for forest tree taxa are mean annual  
 409 daily temperature, and other monthly temperatures, elevation, CHELSA bioclimatic images, monthly  
 410 precipitation and MODIS cloud fraction images. Covariates for lithology and landform classification did  
 411 not feature in the top 20 predictors. It could be that the Global Lithological Map (GLiM) (Hartmann and  
 412 Moosdorf, 2012), which was used to represent changes in lithology, is too general for this scale of work.

413 Fig. 10 illustrates differences between the map of actual distribution of *Fagus sylvatica*, generated by

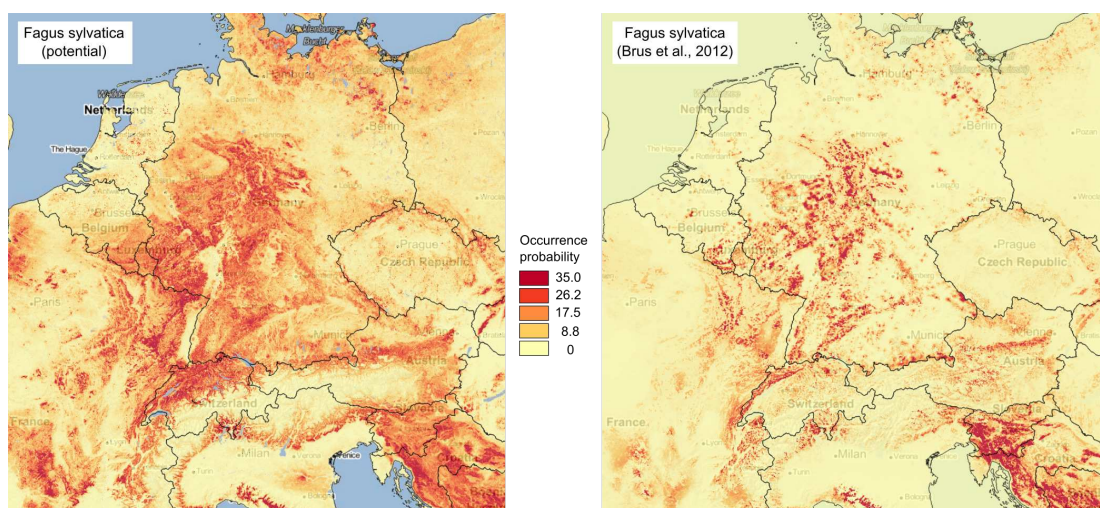


**Figure 10.** Comparison between predicted PNV distribution for *Fagus sylvatica* based on our results, and based on the maps generated by Brus et al. (2012) i.e. showing mapping of the actual distribution of the tree species.

Brus et al. (2012), and our predictions. In this case potential for extending habitat of *Fagus sylvatica* is significant especially over parts of France and Germany.

Correlation analysis (predicted distribution maps) indicates that many forest species are positively correlated especially *Fagus sylvatica* and *Abies alba* and *Populus nigra* and *Salix alba*. High overlap between species probability maps reflects co-existence within communities, and thus provides a way of objectively defining forest communities. Table 2 indicates that even if individual taxa are highly correlated, they can still be mapped reasonably accurately and often with a TPR above 0.80.

# Global monthly FAPAR

The random forest approach also provides the best predictions of potential FAPAR (Fig. 11). The models for FAPAR are highly significant with R-squared around 90 % and RMSE at  $\pm 24$  (original values in the range 0–232 where 235 corresponds to FAPAR=100 %) for the most accurate model based on 5-fold Leave-Location-Out cross-validation. However, unlike with biomes and forest species distributions, the performance of the regression-tree Cubist model shows equal performance with random forest. The most important covariates for predicting FAPAR are total annual precipitation, MODIS cloud fraction images, CHELSA bioclimatic images, and monthly precipitation images. The caret package further suggest that `mtry` parameter for the Random Forest needs to be set higher than the default values for modeling FAPAR. Setting up `mtry > 25` helps reduce the RMSE by about 7–8 %.

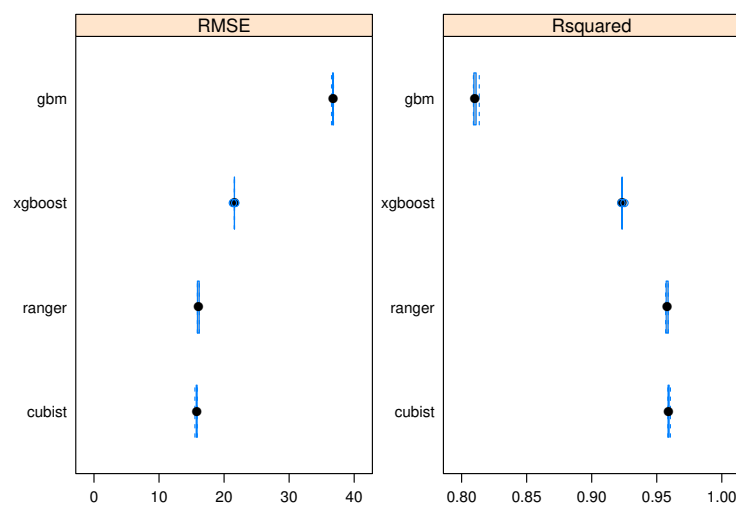


**Figure 11.** Predictive performance of four machine learning algorithms for mapping global distribution of FAPAR ( $N = 180,990$ ). gbm = Generalized Boosted Regression Models, xgboost = Extreme Gradient Boosting, ranger = random forest, cubist = Cubist Regression Models.

Fig. 12 depicts an example of actual vs predicted (PNV based) FAPAR for February in the urban area around São Paulo, where lower actual FAPAR reflects the removal of natural vegetation. Even larger differences between the potential and actual FAPAR are observed in parts of Africa (Fig. 13), likely reflecting land degradation and destruction of vegetation cover. In areas of intensive agricultural production (e.g. Western Australia and Midwest USA), actual FAPAR can be much higher than potential FAPAR under potential natural vegetation in a given month. However this is often a temporal effect, as when PNV FAPAR is aggregated over the whole year, most places modified by human management show actual FAPAR is lower than potential. In Western Australian cropping zones for example, crop fields have higher FAPAR during the winter growing season, but since the fields are bare for most of the year, aggregated annual PNV FAPAR is higher overall. Whilst this pattern may hold for rain-fed agriculture, in intensively irrigated areas the FAPAR of the managed vegetation can be much higher than of the PNV over the whole year, especially in arid and semi-arid areas (e.g. Nile Delta). This supplemental irrigation, plus the fact that total annual precipitation is the most important covariate, indicates that water availability/use



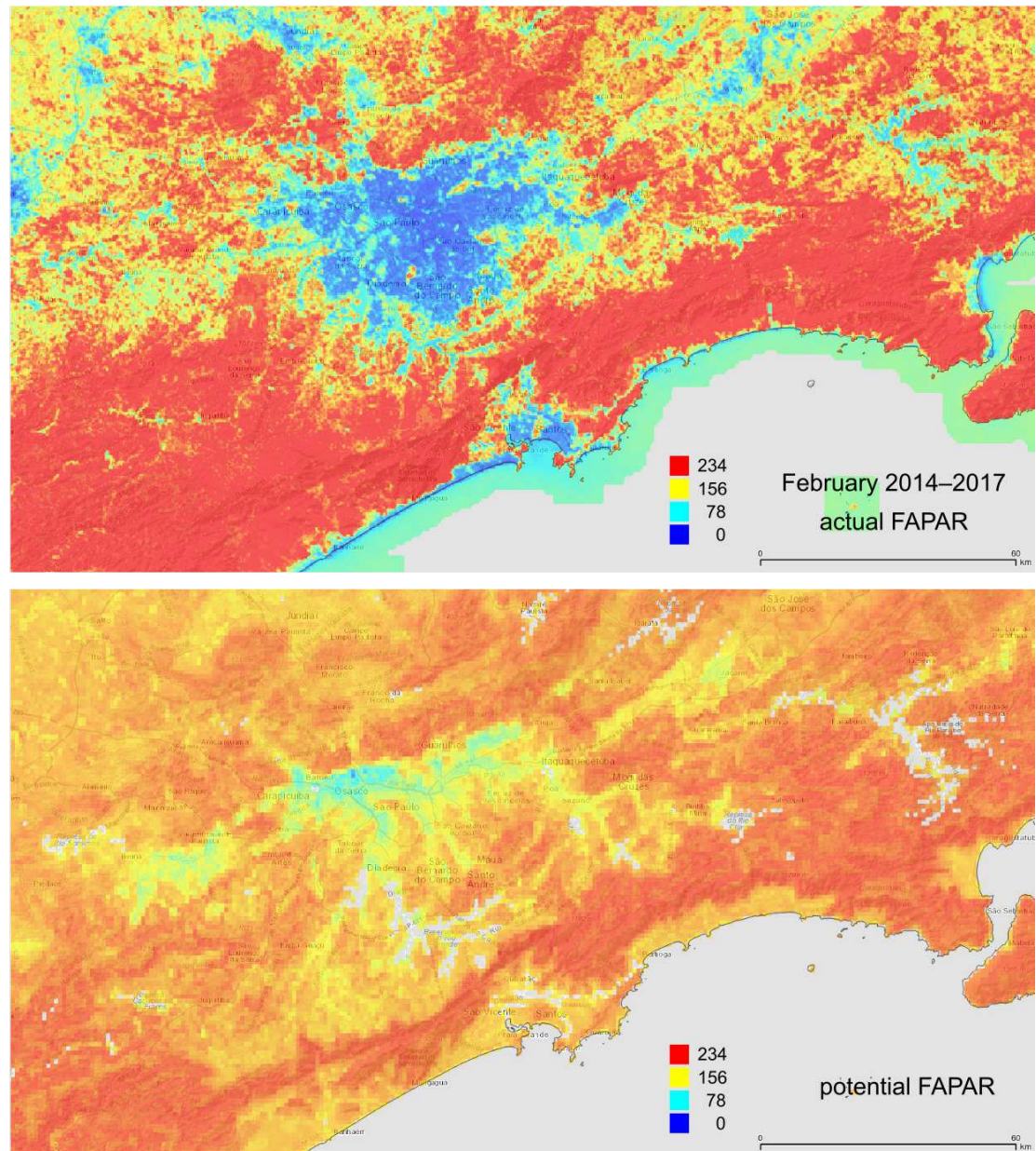


**Figure 12.** Actual (250 m resolution) and predicted (1 km resolution) FAPAR values for February based on the PNV samples: a zoom in area around the city of São Paulo in Brazil.



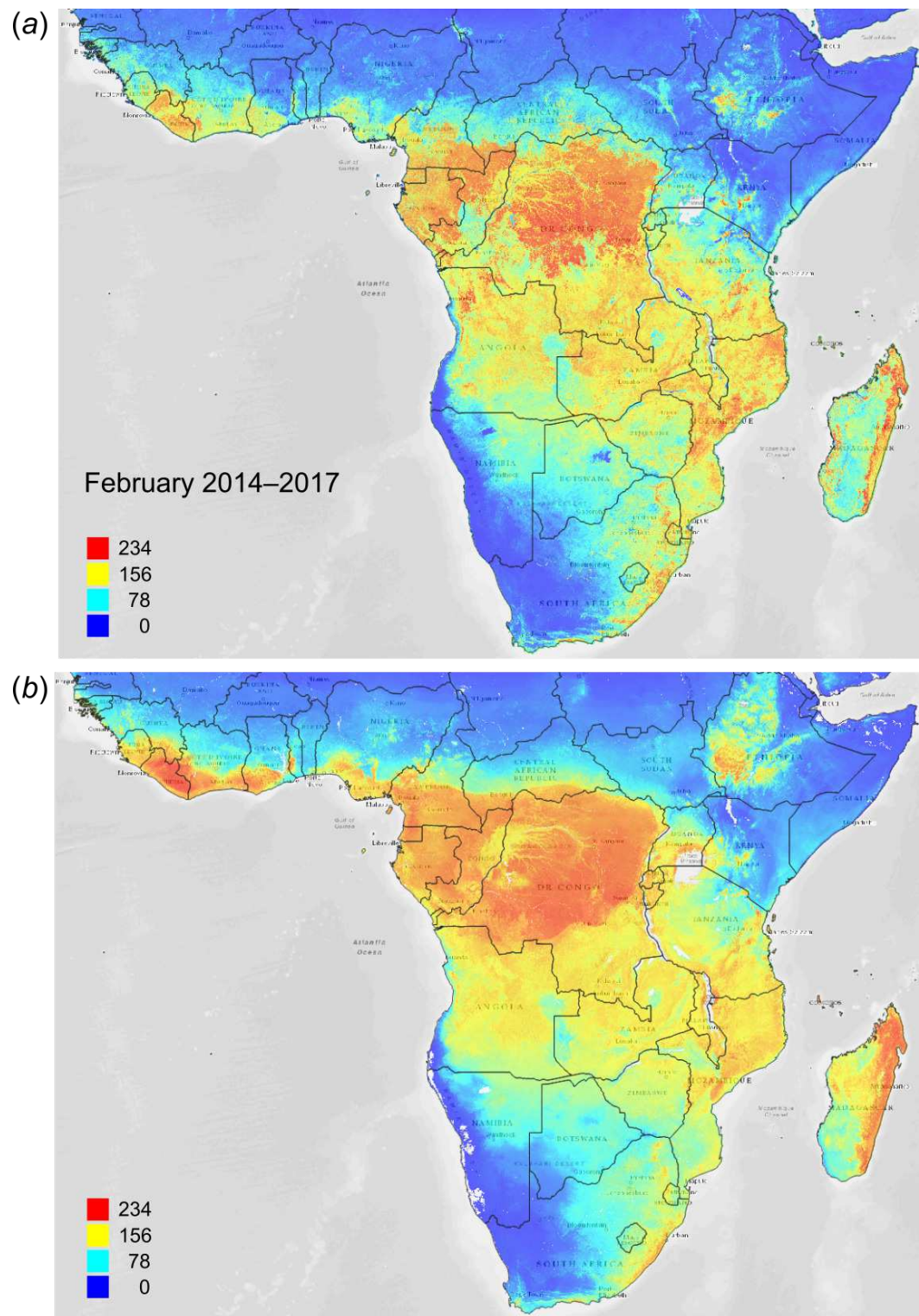


**Figure 13.** FAPAR values for Sub-Saharan Africa: (a) actual (250 m resolution) and (b) predicted (1 km resolution) potential FAPAR values for February.

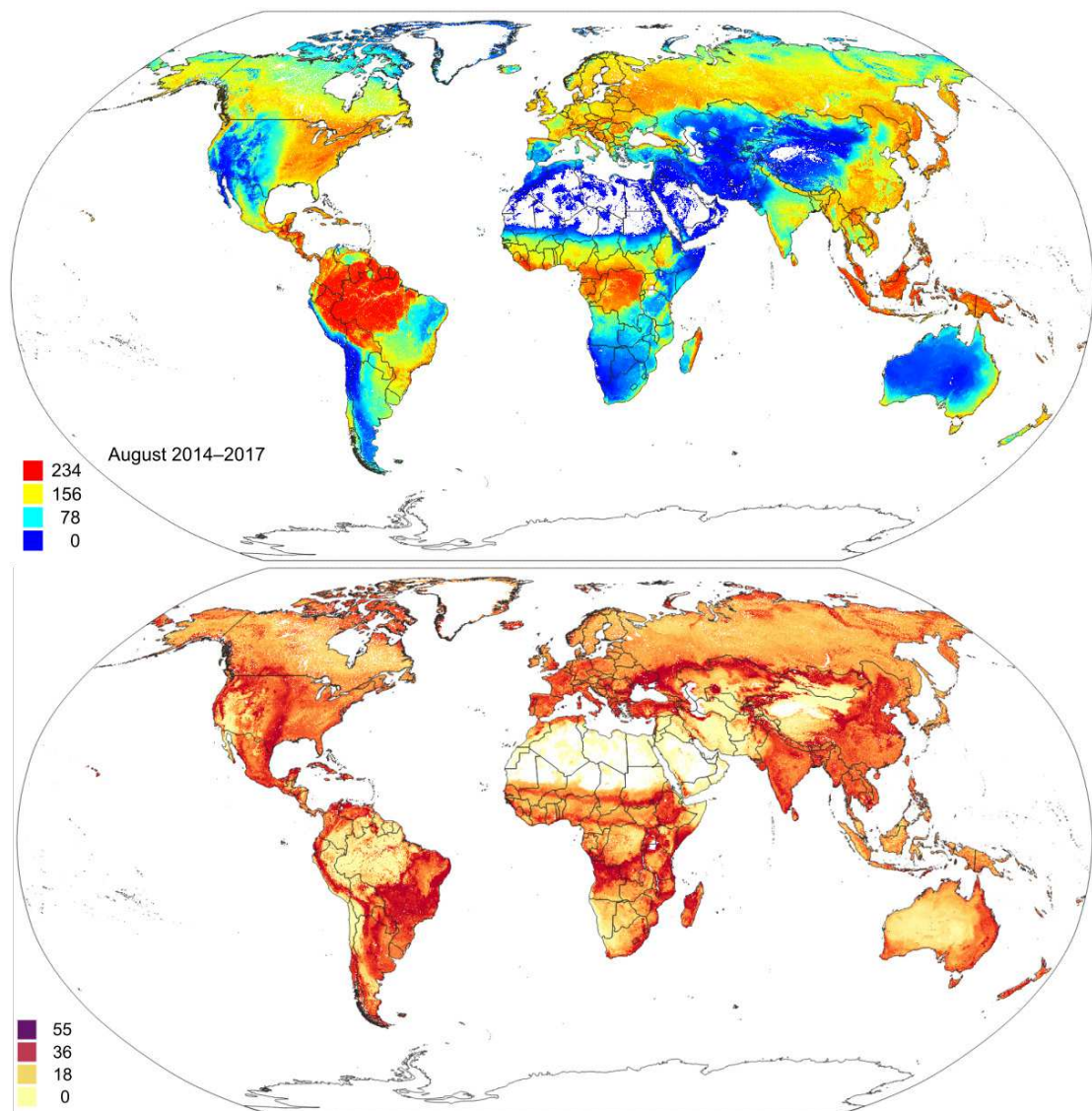


**Figure 14.** Predicted global FAPAR values for August (above) and standard deviation of the prediction error for the map above (below). To convert to percent divide by 253.

444 efficiency is likely the main driver of FAPAR beyond natural conditions.

445 Maps of the standard deviation (s.d.) of the prediction error (Fig. 14) as derived in the ranger package  
 446 by using the quantreg setting (Meinshausen, 2006) provide useful information about model quality  
 447 i.e. where collection of additional points would maximize model improvement and which additional  
 448 covariates could be considered. For example, the highest prediction errors for FAPAR for month August  
 449 occur in the transition areas between tropical forest and savanna areas, and in various biome transition  
 450 zones in Asia.

## DISCUSSION

### Accuracy and reliability of produced PNV maps

Our results of modeling potential spatial distribution of global biomes, potential FAPAR and European forest tree taxa, show that relatively accurate maps of PNV can be produced using existing data and publicly available environmental grids. In the case of the biomes and forest tree taxa case studies, random forest outperforms neural networks, gradient boosting and similar MLA's. However, random forest and Cubist models perform equally well in the case of FAPAR. Accuracy assessment results of our work indicate improvement in product accuracy in terms of higher spatial detail and smaller classification error than the mapping products of [Levvasseur et al. \(2012\)](#) and [Tian et al. \(2016\)](#).

Precipitation, temperature maps and bioclimatic images are consistently the most important covariates in all three case studies. Lithology/parent material are not indicated as significantly important covariates in any of the case studies. This may be because the existing lithologic map ([Hartmann and Moosdorf, 2012](#)) is not detailed enough, and/or it may also reflect the fact that differences in lithology/parent material are important at finer resolutions/scales than those mapped here. Landform and lithology/parent material covariates may be important at local scales, but globally vegetation distribution seems to be dominated by climate. This is not surprising since nutrient availability is also partially controlled by climate and partially by the vegetation itself. Upon visualization of the mapping products however, it was noticed that the influence of topography is visible, especially in the maps of European forest tree taxa, suggesting that DEM derivatives are still important for mapping PNV.

Further improvements in prediction accuracy of global biome may be limited due to:

1. BIOME reconstructions representing the vegetation of an area around the site rather than at the exact point location, since the source of the pollen is on the order of 10–30 km around the site.
2. The ambiguity of reconstructions for about 10 % of the sites, so that maximum accuracy of any prediction technique may not exceed 90 % without additional observation data.
3. The fact that the BIOME reconstruction accuracy is known to be lower at ecotonal boundaries and in mountainous areas because of pollen transport issues, particularly the long-distance transport of tree pollen.
4. The BIOME data set is compiled from many regional reconstructions and all harmonization was done a posteriori, which may have introduced additional noise in the data.

So far, we did not explore opportunities for combining multiple MLA models based on validation data i.e. for doing ensemble predictions, model averages or model stacks. Stacking models can improve upon individual best techniques even up to >30 %, with the additional costs being higher computation loads ([Michailidis, 2017](#)). In our case, the extensive computational load from derivation of models and product predictions had already obtained improved accuracies, making increasing computing loads further still a matter of diminishing returns.

Our models of PNV FAPAR are based on simulated point data and accuracy of how well models represent natural vegetation areas are dependent on the representativeness of the <http://protectedplanet>.



net and <http://intactforests.org> data. Also, many of the world's biomes such as the Mediterranean region and similar, have sustained high levels of human impact in the past and are perhaps under-represented in the <http://protectedplanet.net> data set. Nevertheless, our cross-validation results (Leave-Location-Out method) indicate a good match between training and validation points.

It would be further useful to explore what the performance of the models we used would be if we removed whole continents in the cross-validation process, or at least larger countries such as USA, China, Brazil, Australia, India and/or the South African Republic. For biomes, spatial Cross Validation showed a significant drop in accuracy; taking out some larger country from model training will likely also make difference. We did not explore effects of spatial proximity on mapping forest species and FAPAR as these are very dense point data sets. In addition, FAPAR training points were generated using simple random sampling, so spatial clustering should be non-existent.

#### Possible uses of the produced PNV maps

Newbold et al. (2016) have argued that many terrestrial biomes today have transgressed safe limits for biodiversity, with grasslands being most affected, and tundra and boreal forests least affected. *"Slowing or reversing the global loss of local biodiversity will require preserving the remaining areas of natural (primary) vegetation and, so far as possible, restoring human-used lands to natural."* (Newbold et al., 2016) Roughly half of the difference of around 466 billion tonnes of carbon can be attributed to the clearing of forests and woodlands, mostly for agricultural purposes (Erb et al., 2017). The other half of biomass carbon stock losses is derived from the management effects within a land cover class (Erb et al., 2017). The expansion of agriculture will probably continue in the coming years, leading to decreased biodiversity and soil degradation (Mauser et al., 2015; Molotoks et al., 2017). On the other hand, Griscom et al. (2017) identify reforestation (e.g. biomass restoration) as the largest natural pathway to hold global warming below 2 °C. In that context, accurate maps of PNV could become increasingly useful for assessing the level of land degradation/biomass shortfall against the potential of a site. Such information can also inform selection of optimal steps towards restoring biomass stocks in managed vegetation in ways that better reflect the PNV FAPAR in those areas.

Other uses of PNV maps include assessing the land potential i.e. land use efficiency given the difference between actual and potential vegetation. Consider for example a location in southern Spain called "Altiplano Estepario", which has been identified by the Commonland company (<http://commonland.com>) and partners as a landscape restoration site. Fig. 15 shows results of a spatial query for this location and values of our PNV and PNV FAPAR predictions, in comparison to the actual land cover and actual FAPAR images. The figure shows that the actual FAPAR is as good as PNV FAPAR in February and March but that differences are large in the summer months. Overall, the median and upper FAPAR for this specific location are only 51 % of the PNV FAPAR, so we can say that this site is currently operating at 51 % of the predicted FAPAR capability under PNV. This comparison should also consider that our estimates of FAPAR come with an RMSE of  $\pm 0.085$ . Furthermore, as landscape restoration efforts have recently begun on this site — this work suggests that it ought to be possible to: (a) identify priority areas of PNV FAPAR shortfall, (b) use this information to inform in part the type of restoration strategies used, and (c) monitor the progress of restoration efforts in monthly time steps over several decades. Such

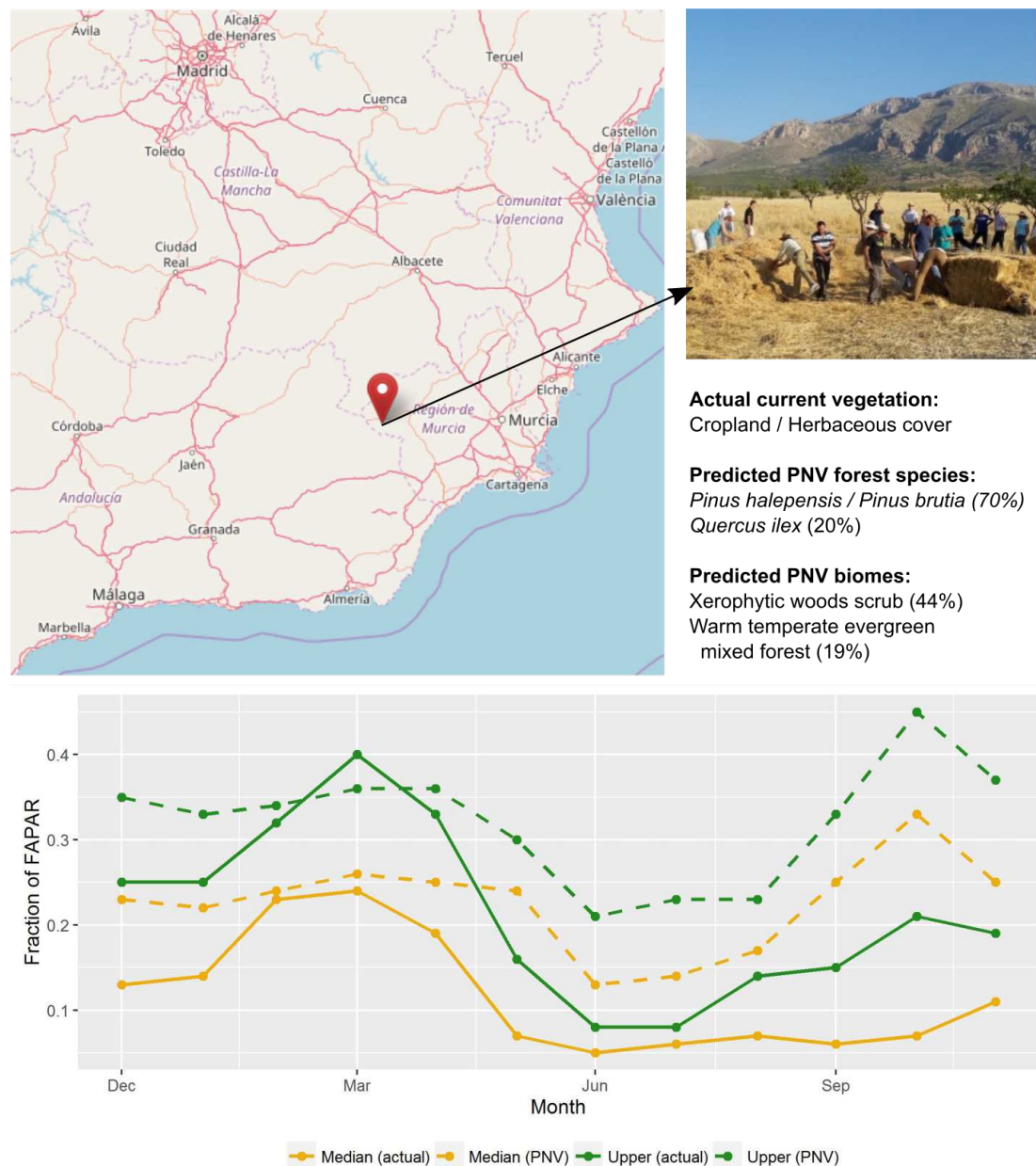


**Figure 15.** Example of comparison between the actual land cover and actual FAPAR curves and our predicted potential natural vegetation (PNV) and predicted PNV FAPAR curves. According to our results, this location in southern Spain (latitude=37.957332, longitude=-2.163181) currently utilizes 51 % of the predicted FAPAR capability under PNV, indicating a substantive short fall in on-site photosynthetically active biomass. Background map source: OpenStreetMap; photograph source: Commonland.

practical measurement, monitoring and verification efforts are required to mobilize further investment in this emerging sector.

Our PNV maps could also be used to estimate soil carbon sequestration and/or evapotranspiration potential, and gains in net primary productivity assuming return of natural vegetation (Fig. 16). Further more, by combining various estimates of potential natural and managed vegetation, one could design the optimal use of land both regionally and globally. Herrick et al. (2013), for example, provide a theoretical

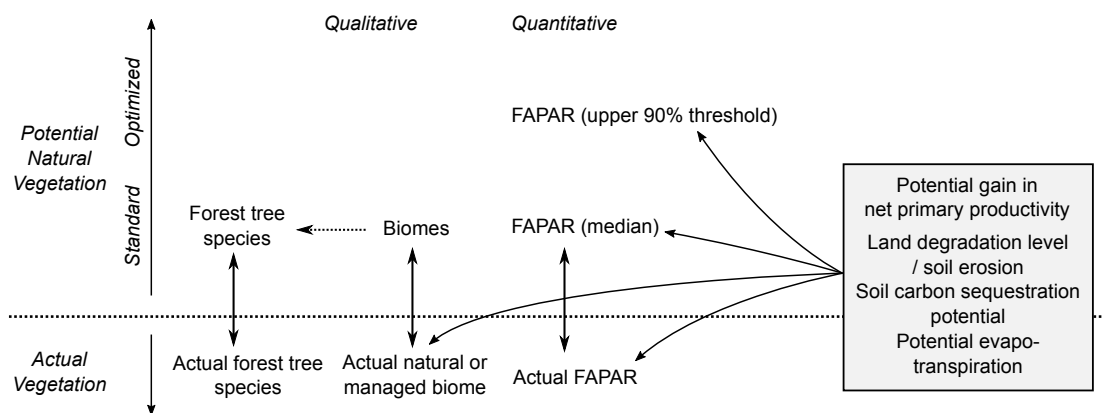


**Figure 16.** Some possible uses of maps of Potential Natural Vegetation.

framework for estimating land potential productivity which could theoretically connect all land owners in the world to share local and regional knowledge.

Maps of PNV for European tree species could also be used as a supplement to the distribution and ecology of tree species produced by San-Miguel-Ayanz et al. (2016) and Brus et al. (2012). PNV type analysis could be made even more quantitative so that even predictions of dendrometric properties of tree species could be produced using similar frameworks. Also, similar PNV mapping algorithms could be used to map the potential canopy height based on the previously estimated map of the global canopy height (Simard et al., 2011).

#### Technical limitations and further challenges

Running Machine Learning Algorithms on larger and larger data is computational demanding; however, by using fully parallelized implementation of random forest in the ranger package, we were able to produce spatial predictions within days. Model fitting and prediction using EU Forest and GBIF data (1.5 million training points) was, however, very memory and time consuming and is not recommended for systems with <126 GiB RAM. In our case, model fitting took several hours even with full parallelization, and final models were >10 GiB in size. Prediction of probabilities took additional 5–6 hours with the current computational set-up. In the future, scalable cloud computing could be used to overcome some of these computational limits.

With enough computing capacity, one could theoretically use all 160 million records of distribution of plant species currently available via GBIF (Meyer et al., 2016) and from other national inventories, and map global distribution of each forest tree species. In Europe the list is very short; globally this list could be quite long (e.g. 60,000 species). The primary problems of using GBIF for PNV mapping will remain however, as these are primarily due to high clustering of points and under-representation of often inaccessible areas with very high biodiversity (Yesson et al., 2007; Meyer et al., 2016). GBIF records have been shown in the past to give biased results (Escribano et al., 2016), so that spatial prediction methods that account for high spatial clustering, i.e. bias in training point representation in both space and time; would need to be developed further to minimize such effects.

## CONCLUSIONS

Although PNV is a hypothetical concept, ground-truth observations can be used to cross-validate PNV models and produce an objective estimate of accuracy. As the prediction accuracy becomes more significant, the reliability of the PNV maps increases. Our analyses show that the highest accuracy for predicting 20 biome classes is about 68 % (33 % with spatial Cross Validation) with the most important predictors being total annual precipitation, monthly temperatures and bioclimatic layers. Predictions of 73 forest tree species had a mapping accuracy of 25 % and with average TPR of 0.69, with the most important predictors being mean annual and monthly temperatures, elevation and monthly cloud fraction. Regression models for FAPAR (monthly images) were most accurate with R-square of 90 % (Leave-Location-Out CV) and with the most important predictors being total annual precipitation, MODIS cloud fraction images, CHELSA bioclimatic layers and month of the year, respectively. Machine learning can be successfully used to model vegetation distribution, and is especially applicable when the training data sets consists of large number of observations and large number of covariates. Extending the coverage of observations of natural and managed vegetation, including through making new ground observations, will allow regular improvements of such PNV maps.

## ACKNOWLEDGMENTS

Funding was provided by The Nature Conservancy and the Doris Duke Charitable Foundation. SPH acknowledges support from the ERC-funded project GC2.0 (Global Change 2.0: Unlocking the past for a clearer future, grant number 694481) and from JPI-Belmont Forum via NERC for the project “PAleao-Constraints on Monsoon Evolution and Dynamics (PACMEDY)”. This research is a contribution to the AXA Chair Programme in Biosphere and Climate Impacts and the Imperial College initiative on Grand Challenges in Ecosystems and the Environment (ICP). Authors are grateful to Karger et al. (2017) for maintaining the CHELSA Climate images, US agencies NASA and USGS for distributing high resolution images of Earth’s atmosphere and the European Copernicus Land program. We are grateful to Mauri et al. (2017) for sharing the EU-Forest — a high-resolution tree occurrence dataset for Europe. We are also grateful to the Open Source software developers of the packages ranger, xgboost, caret, raster, GDAL, SAGA GIS and similar, and without which this work would have not be possible.

## REFERENCES

- Biau, G. and Scornet, E. (2016). A random forest guided tour. *TEST*, 25(2):197–227.
- Bigelow, N. H., Brubaker, L. B., Edwards, M. E., Harrison, S. P., Prentice, I. C., Anderson, P. M., Andreev, A. A., Bartlein, P. J., Christensen, T. R., Cramer, W., et al. (2003). Climate change and arctic ecosystems: 1. vegetation changes north of 55 n between the last glacial maximum, mid-holocene, and present. *Journal of Geophysical Research: Atmospheres*, 108(D19).
- Bischl, B., Lang, M., Kotthoff, L., Schiffner, J., Richter, J., Studerus, E., Casalicchio, G., and Jones, Z. M. (2016). mlr: Machine Learning in R. *Journal of Machine Learning Research*, 17(170):1–5.
- Bohn, U., Zazanashvili, N., and Nakhutsrishvili, G. (2007). The map of the natural vegetation of europe



- 595 and its application in the caucasus ecoregion. *Bulletin of the Georgian National Academy of Sciences*,  
596 175:112–121.
- 597 Borda, M. (2011). *Fundamentals in Information Theory and Coding*. Springer Berlin Heidelberg.
- 598 Breiman, L. (2001). Random forests. *Machine learning*, 45(1):5–32.
- 599 Brenning, A. (2012). Spatial cross-validation and bootstrap for the assessment of prediction rules in  
600 remote sensing: The R package sprrorest. In *2012 IEEE International Geoscience and Remote Sensing*  
601 *Symposium*, pages 5372–5375.
- 602 Brus, D., Hengeveld, G., Walvoort, D., Goedhart, P., Heidema, A., Nabuurs, G., and Gunia, K. (2012).  
603 Statistical mapping of tree species over europe. *European Journal of Forest Research*, 131(1):145–157.
- 604 Carnahan, J. (1989). *Australia natural vegetation: Australia's vegetation in the 1780's*. Australian  
605 Surveying and Land Information Group, Dept. of Administrative Services, Queensland, AU.
- 606 Chen, T. and Guestrin, C. (2016). XGBoost: A Scalable Tree Boosting System. In *Proceedings of the*  
607 *22Nd ACM SIGKDD International Conference on Knowledge Discovery and Data Mining*, KDD '16,  
608 pages 785–794, New York, NY, USA. ACM.
- 609 Conrad, O., Bechtel, B., Bock, M., Dietrich, H., Fischer, E., Gerlitz, L., Wehberg, J., Wichmann, V., and  
610 Böhner, J. (2015). System for automated geoscientific analyses (saga) v. 2.1.4. *Geoscientific Model*  
611 *Development*, 8(7):1991–2007.
- 612 Cutler, D. R., Edwards, T. C., Beard, K. H., Cutler, A., Hess, K. T., Gibson, J., and Lawler, J. J. (2007).  
613 Random forests for classification in ecology. *Ecology*, 88(11):2783–2792.
- 614 Elith, J. and Leathwick, J. R. (2009). Species distribution models: ecological explanation and prediction  
615 across space and time. *Annual Review of Ecology, Evolution, and Systematics*, 40(1):677.
- 616 Erb, K.-H., Kastner, T., Plutzer, C., Bais, A. L. S., Carvalhais, N., Fetzel, T., Gingrich, S., Haberl, H.,  
617 Lauk, C., Niedertscheider, M., et al. (2017). Unexpectedly large impact of forest management and  
618 grazing on global vegetation biomass. *Nature*.
- 619 Escribano, N., Ariño, A. H., and Galicia, D. (2016). Biodiversity data obsolescence and land uses changes.  
620 *PeerJ*, 4:e2743.
- 621 Fan, Y., Li, H., and Miguez-Macho, G. (2013). Global patterns of groundwater table depth. *Science*,  
622 339(6122):940–943.
- 623 Fluet-Chouinard, E., Lehner, B., Rebelo, L.-M., Papa, F., and Hamilton, S. K. (2015). Development of a  
624 global inundation map at high spatial resolution from topographic downscaling of coarse-scale remote  
625 sensing data. *Remote Sensing of Environment*, 158:348–361.
- 626 Friedman, J. H. (2002). Stochastic gradient boosting. *Computational Statistics & Data Analysis*,  
627 38(4):367–378.
- 628 Griscom, B. W., Adams, J., Ellis, P. W., Houghton, R. A., Lomax, G., Miteva, D. A., Schlesinger, W. H.,  
629 Shoch, D., Siikamäki, J. V., Smith, P., Woodbury, P., Zganjar, C., Blackman, A., Campari, J., Conant,  
630 R. T., Delgado, C., Elias, P., Gopalakrishna, T., Hamsik, M. R., Herrero, M., Kiesecker, J., Landis, E.,  
631 Laestadius, L., Leavitt, S. M., Minnemeyer, S., Polasky, S., Potapov, P., Putz, F. E., Sanderman, J.,  
632 Silvius, M., Wollenberg, E., and Fargione, J. (2017). Natural climate solutions. *Proceedings of the*  
633 *National Academy of Sciences*, 114(44):11645–11650.
- 634 Hansen, M. C., Potapov, P. V., Moore, R., Hancher, M., Turubanova, S., Tyukavina, A., Thau, D., Stehman,

- 635 S., Goetz, S., Loveland, T., et al. (2013). High-resolution global maps of 21st-century forest cover  
636 change. *science*, 342(6160):850–853.
- 637 Harrison, S., Yu, G., Takahara, H., and Prentice, I. (2001). Plant diversity and palaeovegetation in east  
638 asia. *Nature*, 413:129–130.
- 639 Harrison, S. P. and Bartlein, P. (2012). Chapter 14 — records from the past, lessons for the future: What  
640 the palaeorecord implies about mechanisms of global change. In Henderson-Sellers, A. and McGuffie,  
641 K., editors, *The Future of the World's Climate (Second Edition)*, pages 403 – 436. Elsevier, Boston,  
642 second edition edition.
- 643 Hartmann, J. and Moosdorf, N. (2012). The new global lithological map database GLiM: A representation  
644 of rock properties at the Earth surface. *Geochemistry, Geophysics, Geosystems*, 13(12):n/a–n/a.
- 645 Hengl, T., Nussbaum, M., Wright, M. N., and Heuvelink, G. B. (2018). Random forest as a generic frame-  
646 work for predictive modeling of spatial and spatio-temporal variables. *PeerJ Preprints*, 6:e26693v1.
- 647 Herrick, J. E., Urama, K. C., Karl, J. W., Boos, J., Johnson, M.-V. V., Shepherd, K. D., Hempel, J.,  
648 Bestelmeyer, B. T., Davies, J., Guerra, J. L., et al. (2013). The global land-potential knowledge system  
649 (landpks): Supporting evidence-based, site-specific land use and management through cloud computing,  
650 mobile applications, and crowdsourcing. *Journal of Soil and Water Conservation*, 68(1):5A–12A.
- 651 Hijmans, R. J. and Elith, J. (2018). *Species distribution modeling with R*. Environmental Science and  
652 Policy, University of California.
- 653 Karger, D. N., Conrad, O., Böhrner, J., Kawohl, T., Kreft, H., Soria-Auza, R. W., Zimmermann, N. E.,  
654 Linder, H. P., and Kessler, M. (2017). Climatologies at high resolution for the earth's land surface areas.  
655 *Scientific data*, 4:170122.
- 656 Kuhn, M. (2008). Building Predictive Models in R Using the caret Package. *Journal of Statistical*  
657 *Software*, 28(1):1–26.
- 658 Kuhn, M. and Johnson, K. (2013). *Applied predictive modeling*. Springer.
- 659 Kuhn, M., Weston, S., Keefer, C., Coulter, N., and Quinlan, R. (2014). *Cubist: rule-and instance-based*  
660 *regression modeling*. R package version 0.0.
- 661 Leong, M. and Roderick, G. K. (2015). Remote sensing captures varying temporal patterns of vegetation  
662 between human-altered and natural landscapes. *PeerJ*, 3:e1141.
- 663 Levavasseur, G., Vrac, M., Roche, D., and Paillard, D. (2012). Statistical modelling of a new global  
664 potential vegetation distribution. *Environmental Research Letters*, 7(4):044019.
- 665 Marchant, R., Cleef, A., Harrison, S., Hooghiemstra, H., Markgraf, V., Van Boxel, J., Ager, T., Almeida,  
666 L., Anderson, R., Baied, C., et al. (2009). Pollen-based biome reconstructions for latin america at 0,  
667 6000 and 18 000 radiocarbon years ago. *Climate of the Past*, 5:725–767.
- 668 Marinova, E., Harrison, S. P., Bragg, F., Connor, S., Laet, V., Leroy, S. A., Mudie, P., Atanassova, J.,  
669 Bozilova, E., Caner, H., et al. (2017). Pollen-derived biomes in the eastern mediterranean–black  
670 sea–caspien-corridor. *Journal of Biogeography*.
- 671 Mauri, A., Strona, G., and San-Miguel-Ayanz, J. (2017). EU-Forest, a high-resolution tree occurrence  
672 dataset for Europe. *Scientific data*, 4:160123.
- 673 Mauser, W., Klepper, G., Zabel, F., Delzeit, R., Hank, T., Putzenlechner, B., and Calzadilla, A. (2015).  
674 Global biomass production potentials exceed expected future demand without the need for cropland

- 675 expansion. *Nature communications*, 6:8946.
- 676 Meinshausen, N. (2006). Quantile regression forests. *Journal of Machine Learning Research*, 7(Jun):983–
- 677 999.
- 678 Meyer, C., Weigelt, P., and Kreft, H. (2016). Multidimensional biases, gaps and uncertainties in global
- 679 plant occurrence information. *Ecology Letters*, 19(8):992–1006.
- 680 Michailidis, M. (2017). *Investigating machine learning methods in recommender systems*. PhD thesis,
- 681 UCL (University College London).
- 682 Molotoks, A., Kuhnert, M., Dawson, T. P., and Smith, P. (2017). Global Hotspots of Conflict Risk between
- 683 Food Security and Biodiversity Conservation. *Land*, 6(4).
- 684 Newbold, T., Hudson, L. N., Arnell, A. P., Contu, S., De Palma, A., Ferrier, S., Hill, S. L., Hoskins,
- 685 A. J., Lysenko, I., Phillips, H. R., et al. (2016). Has land use pushed terrestrial biodiversity beyond the
- 686 planetary boundary? a global assessment. *Science*, 353(6296):288–291.
- 687 Omernik, J. M. (1987). Ecoregions of the conterminous united states. *Annals of the Association of*
- 688 *American geographers*, 77(1):118–125.
- 689 Pekel, J.-F., Cottam, A., Gorelick, N., and Belward, A. S. (2016). High-resolution mapping of global
- 690 surface water and its long-term changes. *Nature*.
- 691 Pickett, E. J., Harrison, S. P., Hope, G., Harle, K., Dodson, J. R., Peter Kershaw, A., Colin Prentice,
- 692 I., Backhouse, J., Colhoun, E. A., D’Costa, D., et al. (2004). Pollen-based reconstructions of biome
- 693 distributions for australia, southeast asia and the pacific (seapac region) at 0, 6000 and 18,000 14c yr
- 694 bp. *Journal of Biogeography*, 31(9):1381–1444.
- 695 Potapov, P., Laestadius, L., and Minnemeyer, S. (2011). *Global Map of Potential Forest Cover*. World
- 696 Resources Institute.
- 697 Potapov, P., Yaroshenko, A., Turubanova, S., Dubinin, M., Laestadius, L., Thies, C., Aksenov, D., Egorov,
- 698 A., Yesipova, Y., Glushkov, I., et al. (2008). Mapping the world’s intact forest landscapes by remote
- 699 sensing. *Ecology and Society*, 13(2).
- 700 Prentice, I. C. and Jolly, D. (2000). Mid-holocene and glacial-maximum vegetation geography of the
- 701 northern continents and africa. *Journal of Biogeography*, 27(3):507–519.
- 702 Ridgeway, G. (2017). *gbm: generalized boosted regression models*. R package version 1.6-3.1.
- 703 Ripley, B. and Venables, W. (2017). *nnet: Feed-Forward Neural Networks and Multinomial Log-Linear*
- 704 *Models*. R package version 7.3-12.
- 705 San-Miguel-Ayanz, J., de Rigo, D., Caudullo, G., Houston Durrant, T., and Mauri, A. (2016). *European*
- 706 *Atlas of forest tree species*. European Commission, Joint Research Centre.
- 707 Shannon, C. E. (1949). Communication in the presence of noise. *Proceedings of the IRE*, 37(1):10–21.
- 708 Simard, M., Pinto, N., Fisher, J. B., and Baccini, A. (2011). Mapping forest canopy height globally with
- 709 spaceborne lidar. *Journal of Geophysical Research: Biogeosciences*, 116(G4):NA.
- 710 Sing, T., Sander, O., Beerenwinkel, N., and Lengauer, T. (2005). ROCR: visualizing classifier performance
- 711 in R. *Bioinformatics*, 21(20):3940–3941.
- 712 Sing, T., Sander, O., Beerenwinkel, N., and Lengauer, T. (2016). *ROCR: Visualizing the Performance of*
- 713 *Scoring Classifiers*. R package version 1.0.7.
- 714 Tian, H., Lu, C., Ciais, P., Michalak, A. M., Canadell, J. G., Saikawa, E., Huntzinger, D. N., Gurney,

- 715 K. R., Sitch, S., Zhang, B., et al. (2016). The terrestrial biosphere as a net source of greenhouse gases  
716 to the atmosphere. *Nature*, 531(7593):225–228.
- 717 Veloso, H. P., Oliveira-Filho, L., Vaz, A., Lima, M., Marquete, R., and Brazao, J. (1992). Manual técnico  
718 da vegetação brasileira.
- 719 Venables, W. N. and Ripley, B. D. (2002). *Modern applied statistics with S*. Springer-Verlag, New York,  
720 4th edition.
- 721 Wilson, A. M. and Jetz, W. (2016). Remotely sensed high-resolution global cloud dynamics for predicting  
722 ecosystem and biodiversity distributions. *PLOS Biology*, 14(3):1–20.
- 723 Wright, M. N. and Ziegler, A. (2016). ranger: A Fast Implementation of Random Forests for High  
724 Dimensional Data in C++ and R. *Journal of Statistical Software*, page 18.
- 725 Yesson, C., Brewer, P. W., Sutton, T., Caithness, N., Pahwa, J. S., Burgess, M., Gray, W. A., White, R. J.,  
726 Jones, A. C., Bisby, F. A., and Culham, A. (2007). How Global Is the Global Biodiversity Information  
727 Facility? *PLoS ONE*, 2(11):e1124.